The neural basis of quantity discrimination in mice

Jikan Peng[1,2,3], Dong Yang[2,3], Chenshi Xu[2,3,4], and Tian Xu[2,3,5*]
[1]School of Medicine, Zhejiang University, Hangzhou, Zhejiang, China
[2]Key Laboratory of Growth Regulation and Translation Research of Zhejiang Province, School of Life Sciences,
Westlake University, Hangzhou, Zhejiang, China
[3]Westlake Laboratory of Life Sciences and Biomedicine, Hangzhou, Zhejiang, China
[4]Fudan University, Shanghai, China
[5]Department of Genetics, Yale University School of Medicine, New Haven, USA
*Correspondence: xutian@westlake.edu.cn

Abstract
Quantity discrimination, the ability to identify preferable sizes or amounts of subjects, is well-documented across humans and animals, yet its underlying neural mechanisms remain poorly understood. Here, we report that mice exhibit an innate quantity discrimination behavior for food amounts, consistent with the Weber-Fechner law. Inhibition of the Posterior Parietal Cortex (PPC), but not other cortex regions, disrupts this behavior. Two-photon analysis reveals that selected neurons with preferential activities or "Number Neurons" are detected at a given time; however, these neurons are not correlated with quantity discrimination behavior and alter their preferential identities over time. Furthermore, inhibition of other cortex regions with "Number Neurons" does not affect quantity discrimination. Conversely, the PPC neuronal population changes synchronous firing levels, which correlates with quantity discrimination behavior and could be explained by a Neural Entropy model. Together, our study identifies a central role of the PPC in quantity discrimination, providing a neuronal population model of synchronous firing for quantity discrimination coding.

Introduction
Quantity discrimination is an essential ability for human and animal survival. This ability enables individuals to judge different sizes or amounts of subjects for the preferable conditions. For example, human infants and chimpanzees choose a larger piece of cracker over a smaller one[1,2]. Similarly, when presented with prey of different sizes, cats and cuttlefish select the larger one[3,4]. Furthermore, when offered a choice between two sets of crackers with different amounts, human infants choose the set with more crackers[1]. Similar behaviors were also observed in chimpanzees, dogs, monkeys, mongoose lemurs, sea lions, salamanders, and ungulate species[5-11]. In addition to food, quantity discrimination behavior is also important when judging conspecifics, predators, and other environmental cues[12-18]. Therefore, quantity discrimination allows individuals to identify preferable conditions of sizes or amounts, which are crucial for animal survival. Moreover, the presence of quantity discrimination behaviors from humans to fish suggests conserved mechanisms throughout evolution.

Brain imaging studies has identified potential cortex regions associated with quantity discrimination in humans when individuals were subjected to judging different numbers of dots or numerical symbols[19-30]. In addition to the sensory cortex for processing inputs, the Prefrontal Cortex (PFC) and the Posterior Parietal Cortex (PPC) were identified in these fMRI studies for quantity discrimination. In addition to brain imaging studies, electrophysiological recording in monkeys has also identified neuronal activity within the PFC, the PPC, as well as the Anterior Inferior Temporal Cortex (aITC), when

animals were trained to recognize images with the same number of dots[31-33]. Moreover, these electrophysiological studies identified a group of neurons in these three regions exhibiting activities preferentially tuned towards a given number of dots[31-33]. Thereafter, it has been proposed that these specific neurons, or the "Number Neurons", represent an abstract code for numbers[34-36].

Here, we report the establishment of a food-based assay for quantity discrimination in the model organism, the mouse. Furthermore, we have identified the functional involvement of the PPC in quantity discrimination through inhibitory chemogenetics. Finally, we have analyzed neuronal activity in the PPC using two-photon imaging during quantity discrimination. Our analysis does not support the "Number Neurons" coding hypothesis, and instead, reveals that the PPC neuronal population exhibits changes in synchronous firing levels, which correlates with quantity discrimination behavior.

Results

A food-based assay reveals quantity discrimination behavior in mice

We investigated whether mice have an innate capacity of quantity discrimination when presented with different amounts of food. In the food-based assay, individual naïve adult mice were introduced into an open field arena containing designated amounts of food in the two opposing corners (Fig. 1a, b; Methods). The foraging movement of each animal was continuously monitored for one hour and the accumulative time each animal spent within the specific zone with the different amount of food was analyzed. Two representative examples of the foraging behavior were illustrated (Fig. 1c and Extended Data Fig. 1). When presented with 20g versus 80g of food in the assay, significant disparities were observed for the times that individual mice spent in different foraging zones, resulting in measurements of 20.17 ± 2.13% (mean ± s.e.m.) and 67.34 ± 2.80%, respectively (Fig. 1d). Moreover, the amounts of food consumed from the 80g container was approximately twice that from the 20g container (Extended Data Fig. 2a). No disparity was observed when equal amounts of food were presented in the assay (Fig. 1d and Extended Data Fig. 2a). In addition to the C57BL/6J strain, the 129 and the BALB/c strains of mice exhibited similar behavior (Fig. 1e and Extended Data Fig. 2b). Finally, the quantity discrimination behavior was also observed when additional different amounts of food were presented (Fig. 1f and Extended Data Fig. 3). These results revealed that mice can distinguish different amounts of food and show a preference towards more food, exhibiting a true quantity discrimination behavior. Furthermore, the quantity discrimination for amounts of food is an innate behavior in mice without training, facilitating and simplifying future mechanistic studies.

In addition to brain imaging studies, the relationship between the different numbers or ratios of dots and the discriminating ability has been examined in humans of different ages[37]. These studies revealed that human's ability to discriminate dots follows the Weber-Fechner law, which is a general principle in behavioral science describing the relationship between the intensity of the physical stimuli and the perceived strength of these stimuli[38,39]. We therefore examined the relationship between different amounts or ratios of food and the quantity discrimination behavior in mice and confirmed that food quantity discrimination in mice also follows the Weber-Fechner law (Fig. 1f and Extended Data Fig. 2a, 3; Extended Data Table 1). The Weber-Fechner law also specifies a threshold for discriminating distinct stimulus intensities, known as the Weber fraction (ω) indicating the strength of perception ability[38,39]. Our experiments revealed a Weber fraction value of 0.37 for food quantity discrimination in mice (Fig. 1f). Together, these results indicate that the food quantity discrimination behavior in

mice is similar to the ability to discriminate dots in humans and with the ability comparable to 3 year-old humans[37].

Visual input is required for food quantity discrimination in mice

We then explored the sensory modality influencing the food quantity discrimination behavior in mice. We first assessed the contribution of olfactory sensation by inducing temporary anosmia with a chemical agent (Methods). Despite successful induction of olfactory anosmia (Extended Data Fig. 4), the food quantity discrimination behavior was not disrupted in mice (Fig. 1g and Extended Data Fig. 2c). Subsequently, we evaluated the role of tactile sensation by removal of tactile bristles and found that the food quantity discrimination behavior maintained (Fig. 1g and Extended Data Fig. 2c). In contrast, disruption of visual sensation via surgical ablation of retinal ganglion fibers resulted in a loss of the food quantity discrimination in mice (Fig. 1g and Extended Data Fig. 2c). This observation was further confirmed by experiments with visually compromised mice, including FVB/NJ adults with retinal detachment and $Arf^{FL/+}$ transgenic animals with congenital blindness (Fig. 1g and Extended Data Fig. 2c). To underscore the importance of visual cues in food quantity discrimination, we conducted a visual illusion experiment with wild-type animals, in which a plastic block was buried in food in the container with less food, visually aligning it with the container with more food (40g with block, 80g without block). Consistent with experiments of damaged visual system, visual illusion disrupted the food quantity discrimination (Fig. 1d, g, and Extended Data Fig. 2c). These findings revealed that visual input is critical for food quantity discrimination in mice.

The PPC is required for quantity discrimination

We then investigated which brain regions might be functionally required for quantity discrimination in mice. As fMRI imaging and electrophysiological recording in humans and monkeys have revealed associated activities in several cortex regions with quantity discrimination[19-24,31-33], we examined whether the PPC is functionally required for quantity discrimination for food in mice using inhibitory chemogenetics (Extended Data Fig. 5; Methods). We found that inhibition of the PPC eliminated the food quantity discrimination behavior in mice (Fig. 2a and Extended Data Fig. 2d). In contrast, inhibition of the mouse equivalent of aITC, the Postrhinal Cortex (POR), did not disrupt this quantity discrimination behavior (Fig. 2a and Extended Data Fig. 2d). To discern if the disruption of the PPC activity might impact visual sensory function, we conducted a novel object recognition test and confirmed that visual sensory activity was unaffected by the PPC inhibition (Extended Data Fig. 6; Methods). Together, our findings in mice provided the first evidence that the PPC is functionally required for quantity discrimination.

No "Number Neurons" for quantity discrimination

In the electrophysiological studies of monkeys, specific neurons with preferential activities for different number of dots, or the "Number Neurons", were identified in three cortical regions: the PPC, the POR/aITC, and the PFC[31-33]. However, our experiments revealed that inhibition of the POR/aITC did not disrupt quantity discrimination in mice (Fig. 2a). Among the three cortex regions, 30% of the recorded neurons in the PFC are the "Number Neurons", which is much higher than 10% and 5% detected in the PPC and the POR/aITC, respectively[32]. Therefore, to further investigate whether the "Number Neurons" are involved in quantity discrimination, we inhibited

the PFC, which has the most "Number Neurons", and found that this inhibition also did not disrupt quantity discrimination behavior (Fig. 2a and Extended Data Fig. 2d). These findings suggested that the "Number Neurons" may not be required for quantity discrimination.

As the "Number Neurons" were also identified in the PPC[32,33], we decided to conduct a detail examination of the neuronal activity in the PPC during quantity discrimination in mice using two-photon imaging technology. This technology allows one to continuously monitor the activities of more than hundred neurons in each freely moving animal over extended periods[40]. Briefly, we virally expressed the calcium indicator GCaMP6f in the PPC and recorded neuronal activity within layer II/III of the PPC during the food quantity discrimination assay using two-photon microscopy (Fig. 2b and Extended Data Fig. 7a; Methods)[41]. The two-photon imaging data was processed following standard procedures[42-44], and the activities of 7,378 neurons across 48 mice were recorded (Extended Data Table 2 and Extended Data Fig. 8, 9; Methods). Two distinct events in which a mouse moved from one foraging zone to another were identified and used for subsequent decoding analysis (Fig. 2c and Extended Data Fig. 7b; Methods). We did detect about 10% of the PPC neurons showing preferential activities towards either the 20g or 80g of food at a given time (Extended Data Fig. 10a-c; Methods), which is very similar to the results from the electrophysiology studies in monkeys[32,33]. However, when the same neurons were followed at different periods, they had altered their preferential activities toward the different food amounts (Fig. 2d, e and Extended Data Fig. 10d). In other words, the "Number Neurons" had altered their preferential identities. Finally, we examined the "Number Neurons" phenomenon when the animals were presented with the equal amounts of food (20g versus 20g). We found that neurons with preferential activities were still detected at a given time and again such preferential activities changed over time (Fig. 2f, g and Extended Data Fig. 10a-c, e). Together, these results indicated that there are no true "Number Neurons" and argue against the "Number Neuron" coding hypothesis.

The levels of synchronous firing in the PPC neuronal population predict quantity discrimination behavior

As selected neurons with preferential activities fail to explain quantity discrimination, we analyzed the population of the PPC neurons for potential activity pattern predicting quantity discrimination behavior. First, we found that there is no significant difference in the firing magnitude of neurons when the animals were presented with different amounts of food (Extended Data Fig. 11; Methods). We then analyzed the pattern of synchronous firing of the PPC neuronal population during quantity discrimination (Methods). This analysis revealed that significant number of the PPC neurons exhibit synchronous firing, with a Jaccard Index value as high as 0.7 (Fig. 3a; Methods). The average duration of the synchronous firing is 1.95 ± 0.02 seconds (Extended Data Table 2 and Extended Data Fig. 12). Furthermore, we discovered that all the recorded PPC neurons are activated during quantity discrimination and are participated in synchronous firing (Extended Data Fig. 13; Methods). Excitingly, we discovered that the levels of synchronous firing of the PPC neuronal population are changed when animals were presented with different amounts of food. First, when the animals moved from the 20g to the 80g foraging zone, the levels of synchronous firing decreased (Fig. 3b). Conversely, an opposite trend was observed when they transitioned from the 80g to the 20g foraging zone (Fig. 3b). In contrast, no such differences were observed when equal amounts of food were presented (Fig. 3c). Second, unlike previous observations in "Number Neurons", such changes in the levels of synchronous firing persisted over

time (Fig. 3d, e). Finally, when the animals were presented with either 20g or 80g of food, the corresponding levels of synchronous firing were 23.33 ± 0.76% and 16.61 ± 0.75%, respectively (Table 1, Fig. 3f and Extended Data Fig. 14). In contrast, when the animals were presented with the same amount of food (20g versus 20g), the level of synchronous firing remained the same (Table 1, Fig. 3g and Extended Data Fig. 14). Furthermore, when additional different amounts of food were examined (40g, 60g, 70g, and 90g), we discovered that the levels of synchronous firing inversely correlated with the amounts of food (Table 1, Fig. 3h and Extended Data Fig. 14, 15). Together, these data revealed that the PPC neuronal population exhibits significant levels of synchronous firing, and the levels of synchronous firing correlate with the quantity discrimination behavior.

It is intriguing how the levels of synchronous firing in the PPC could code the information for quantity discrimination. The fundamental elements of synchronous firing are the firing or the resting status of individual neurons, which is very similar to the on or the off status of the transistors on the computer chip[45]. The quantity information or other contents coded by the binary statuses of the transistors on a chip is measured by Shannon's Entropy (Fig. 4a; Methods)[46]. By analogy, we proposed a Neural Entropy model to calculate the levels of synchronous firing in the PPC or in any given population of neurons (Fig. 4b; Methods). Specifically, the firing or the resting status of each neuron behaves as a binary coding unit. The aggregation of pairwise synchronous firing for all neurons in the population or the level of synchronous firing could be calculated accordingly following the Neural Entropy model (Fig. 4b; Methods). Using the recorded data of neuronal activities in the PPC during quantity discrimination, we calculated the Neural Entropy values for the 20g or 80g of food quantity discrimination to be 0.14 ± 0.01 or 0.45 ± 0.01 bits, respectively, which is consistent with the quantity discrimination behavior (Fig. 4b). Furthermore, the Neural Entropy calculation based on the levels of synchronous firing for the other different amounts of food also resulted in distinctive values consistent with the outcomes of the behavior (Extended Data Fig. 16). Together, these findings indicated that the levels of synchronous firing in the PPC predicts the quantity discrimination behavior, whose values could be measured by the Neural Entropy model.

Discussion

Quantity discrimination enables individuals to identify preferable sizes or amounts of subjects, such as food, that are essential for animal survival. Here, we have established the first food-based assay to study quantity discrimination behavior in a model organism. Different strains of mice display an innate quantity discrimination ability for different amounts of food. Our analysis revealed that this ability for food amounts relies on the stimulus input from visual perception. Furthermore, the relationship between stimulus intensity of food amounts and quantity discrimination in mice follows the Weber-Fechner law, which is consistent with the results in humans for identifying different numbers or dots[37,38,47]. Compared to humans, monkeys, and crows, which have been used to study quantity discrimination or numeracy in the past, the mouse as a model organism offers many advantages for experimental manipulation and mechanistic exploration. Finally, different from discriminating dot numbers or sound beats in the past studies, quantity discrimination for different amounts of food is an innate behavior without training. Such an innate assay offers unique advantages in reducing the complexity and confounding factors introduced by learning and training.

Multiple cortex regions have been previously suggested to be involved in quantity discrimination through fMRI imaging and electrophysiological recording for

discriminating dot numbers or numerical symbols in humans and monkeys[19-33]. Using inhibitory chemogenetics, we have now shown that inhibition of the PPC, but not the PFC or the POR/aITC, blocks food quantity discrimination in mice. Additionally, our companion study has shown that patients with surgery involved in the PPC fail in quantity discrimination and there is a genetic association between the PPC and intelligence for quantity discrimination[48]. Overall, our findings have, for the first time, identified that the PPC is functionally required for quantity discrimination. Recent studies have shown that the PPC is also involved in navigation decision[49-51]. Specifically, mice were trained for navigation decision in discriminative responses to images of dots, stripes, or different sound tones[52-68]. Together, our work and the previous studies indicate that the PPC is responsible for discriminative decisions.

The electrophysiological recording of monkeys for recognizing the number of dots identified the existence of specific neurons exhibiting activities preferential towards specific numbers of dots, which led to the hypothesis that these "Number Neurons" represent an abstract code for numbers or quantity discrimination[31-36]. However, multiple lines of evidence from this work and the navigation decision studies are against the existence of such "Number Neurons" and their role in quantity discrimination. First, our results showed that inhibition of the PFC or the POR/aITC, two regions containing "Number Neurons"[31-33], did not affect quantity discrimination. Second, when the animals were presented with the equal amounts of food, neurons with different preferential activities were still detected. Third, and more importantly, our experiments revealed that the neurons with preferential activities alter their preferential identities as two-photon imaging continuously monitored the activities for the same neurons over time. Similar results were also reported in the navigation decision studies, in which two-photon analysis revealed that the neurons in the PPC with preferential activities were detected at a given time and such preferential activities altered over time[56,59,64]. Therefore, there is no true "Number Neurons". Furthermore, the "Number Neurons" coding hypothesis also has shortcomings in theoretical consideration. First, if it requires a special group of "Number Neurons" to code for each number, a vast number of neurons are needed to code for many numbers. By contrast, we and others have found that the levels of synchronous firing or the states of the PPC neuronal population discriminates different quantity or navigation conditions. In other words, the PPC functions by determining differences in quantities or conditions in the given situations, which could be applied to numerous settings. The most unsettlingly issue is the "Number Neurons" coding hypothesis does not explain which number is bigger, which is essential to quantity discrimination in determining the preferable condition(s) for animal survival. Together, both experimental evidence and theoretical considerations do not support the "Number Neurons" coding hypothesis.

To elucidate the underlying neural basis for quantity discrimination, our analysis revealed that there is no significant difference in either the number of firing neurons or the firing magnitude when the animals were presented with different amounts of food. Instead, we found that all neurons in the PPC exhibit activities during quantity discrimination and significant number of them display synchronous firing. Interestingly, we have discovered that the levels of synchronous firing of the PPC neuronal population correlate with the quantity discrimination behavior. Therefore, our results indicate that the coding of the PPC for quantity discrimination does not depend on the number of firing neurons, the firing magnitude, or special neurons with preferential activities, but rather on the levels of synchronous firing of the PPC neuronal population. The fundamental elements of synchronous firing are the firing and resting binary statuses of individual neurons in a neuronal population. Binary coding systems have been utilized

throughout human history, including the Chinese Bagua, Africa Ifa, Braille for visually impaired, and the transistors in computer chips[45,69]. The information content for the computer chip(s) is coded by the binary statues of the collection of the transistors and calculated by Shannon's Entropy[46]. In analogy, we have proposed a Neural Entropy model for calculating the information content of synchronous firing of a neuronal population and discovered that the Neural Entropy values of synchronous firing of the PPC neuronal population could predict the quantity discrimination behavior. It is intriguing to consider whether similar coding system operates in other neuronal populations of the brain. Finally, it is fascinating to speculate whether forthcoming studies of the coding and energy strategies of the PPC could facilitate the design of future chips and computers.

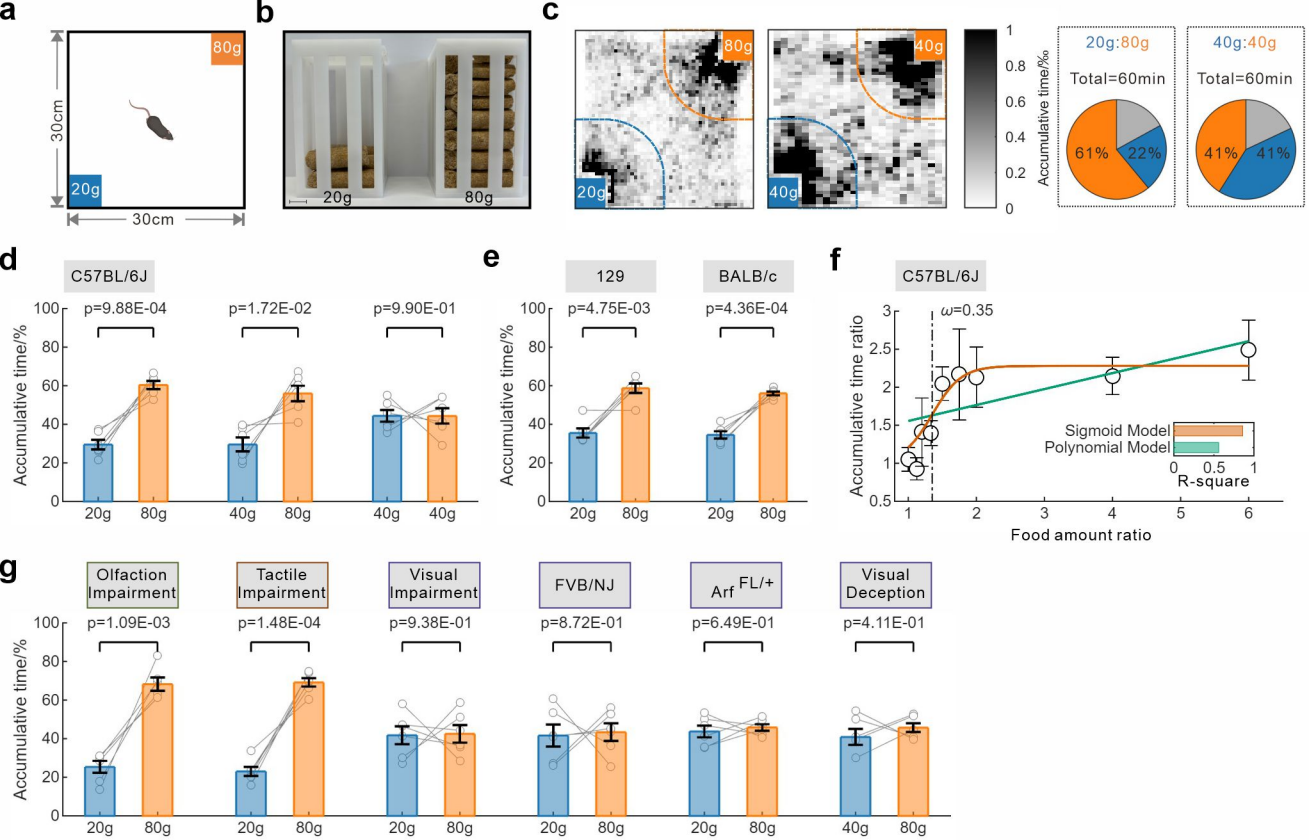
a
80g
30cm
20g
30cm
b
20g
80g
c
80g
20g
40g
40g
1
0.8
0.6
0.4
0.2
0
Accumulative time/‰
20g:80g
Total=60min
61%
22%
40g:40g
Total=60min
41%
41%
d
C57BL/6J
p=9.88E-04
p=1.72E-02
p=9.90E-01
Accumulative time/%
20g
80g
40g
80g
40g
40g
e
129
BALB/c
p=4.75E-03
p=4.36E-04
Accumulative time/%
20g
80g
20g
80g
f
C57BL/6J
ω=0.35
Accumulative time ratio
Food amount ratio
Sigmoid Model
Polynomial Model
R-square
0
0.5
1
g
Olfaction Impairment
Tactile Impairment
Visual Impairment
FVB/NJ
Arf FL/+
Visual Deception
p=1.09E-03
p=1.48E-04
p=9.38E-01
p=8.72E-01
p=6.49E-01
p=4.11E-01
Accumulative time/%
20g
80g
20g
80g
20g
80g
20g
80g
20g
80g
40g
80g

Fig. 1| Quantity discrimination for food amounts in mice. a, Schematic representation of different amounts of food in an open arena in a food-based quantity discrimination assay. **b**, Representative food containers holding either 20g or 80g of food. Scale bar, 1cm. **c**, Tracking map illustrating the percentage of time the animal spent in each foraging zone (20g versus 80g, or 40g versus 40g). **d**, **e**, Quantity discrimination behavior for different ratios of food amounts in the C57BL/6J (**d**), 129 and BALB/c (**e**) mice. **f**, Quantity discrimination behavior for food amounts in mice follows the Weber-Fechner law. The relationship of the food amount ratio versus the accumulative time ratio fits with either the sigmoid (yellow line) or the polynomial (green line) model. The corresponding R-square values indicate model fitness, while the estimated Weber fraction (ω) is marked by the dotted line. **g**, Quantity discrimination behavior following block of specific sensory inputs including chemical-induced olfactory anosmia, tactile sensory deprivation by whisker removal, or visual impairment due to crushing of optic nerves, retinal detachment, blindness, or visual deception of food amount. For **d**, **e** and **g**, two-tailed paired t-test; mean and s.e.m. are shown; dots manifest data from individual mice (N=6).

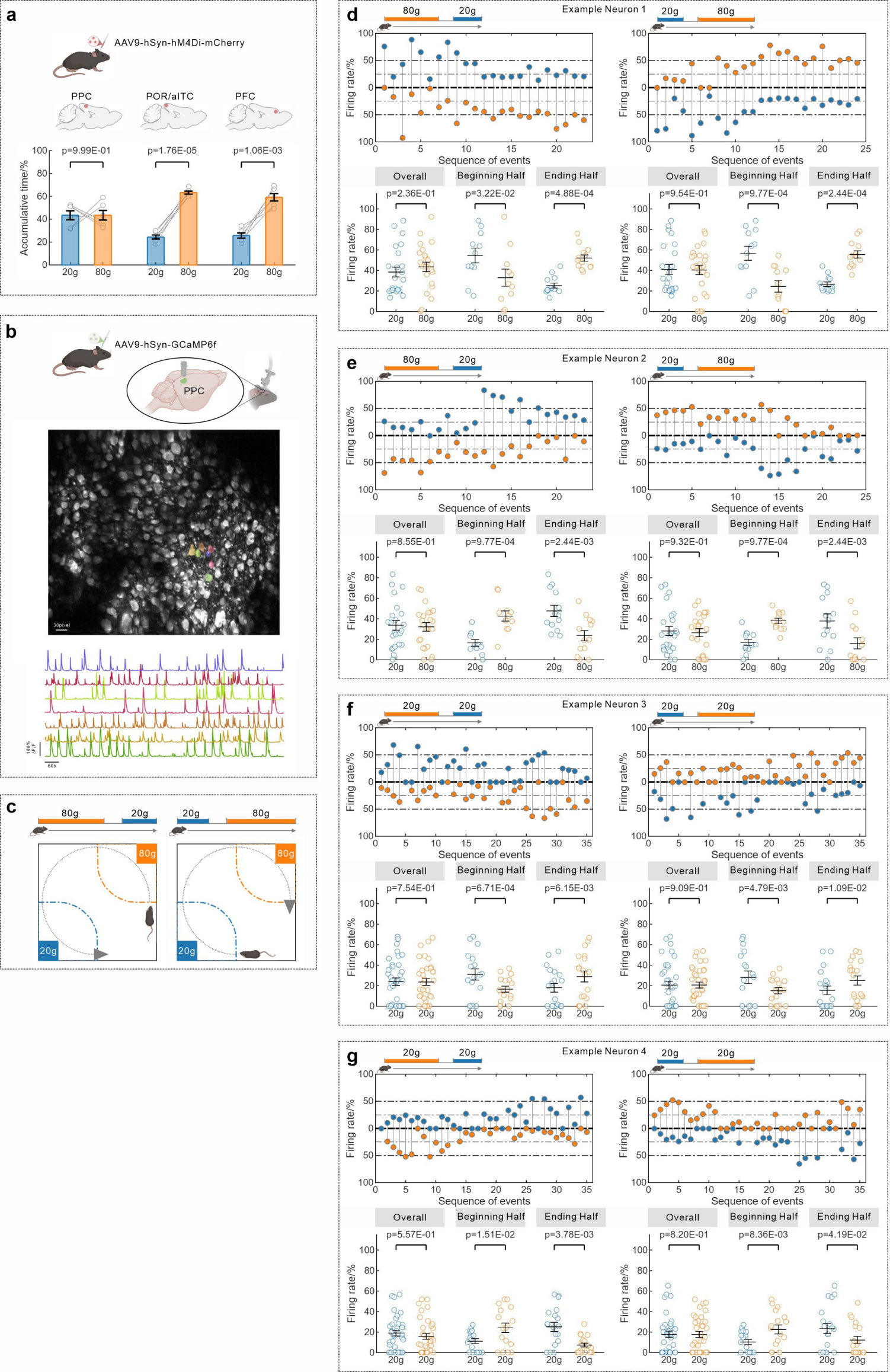
a
AAV9-hSyn-hM4Di-mCherry
PPC
POR/aITC
PFC
p=9.99E-01
p=1.76E-05
p=1.06E-03
Accumulative time/%
20g
80g
b
AAV9-hSyn-GCaMP6f
PPC
30pixel
60s
c
80g
20g
d
Example Neuron 1
Firing rate/%
Sequence of events
Overall
Beginning Half
Ending Half
p=2.36E-01
p=3.22E-02
p=4.88E-04
p=9.54E-01
p=9.77E-04
p=2.44E-04
e
Example Neuron 2
p=8.55E-01
p=9.77E-04
p=2.44E-03
p=9.32E-01
p=9.77E-04
p=2.44E-03
f
Example Neuron 3
p=7.54E-01
p=6.71E-04
p=6.15E-03
p=9.09E-01
p=4.79E-03
p=1.09E-02
g
Example Neuron 4
p=5.57E-01
p=1.51E-02
p=3.78E-03
p=8.20E-01
p=8.36E-03
p=4.19E-02

Fig. 2| The involvement of the PPC for quantity discrimination. a, Quantity discrimination behavior in mice following the inhibition of neuronal activity in the PPC, the POR/aITC, or the PFC. Two-tailed paired t-test; mean and s.e.m. are shown; dots manifest data from individual mice (N=6). **b**, Two-photon imaging analysis for neuronal activity in layer II/III of the PPC during the quantity discrimination assay. Representative calcium signals from the PPC neurons are shown. **c**, Two distinct events in which a mouse transitioned between two foraging zones. **d**, **e**, Altered preferential activities of two typical neurons in the PPC during the quantity discrimination assay for 20g versus 80g of food at either the beginning or the ending half. **f**, **g**, Preferential activities of two typical neurons in the PPC during the quantity discrimination assay for 20g versus 20g of food at either the beginning or the ending half. For **d**-**g**, two-tailed Wilcoxon signed-rank test; mean and s.e.m. are shown; dots manifest data from individual events.

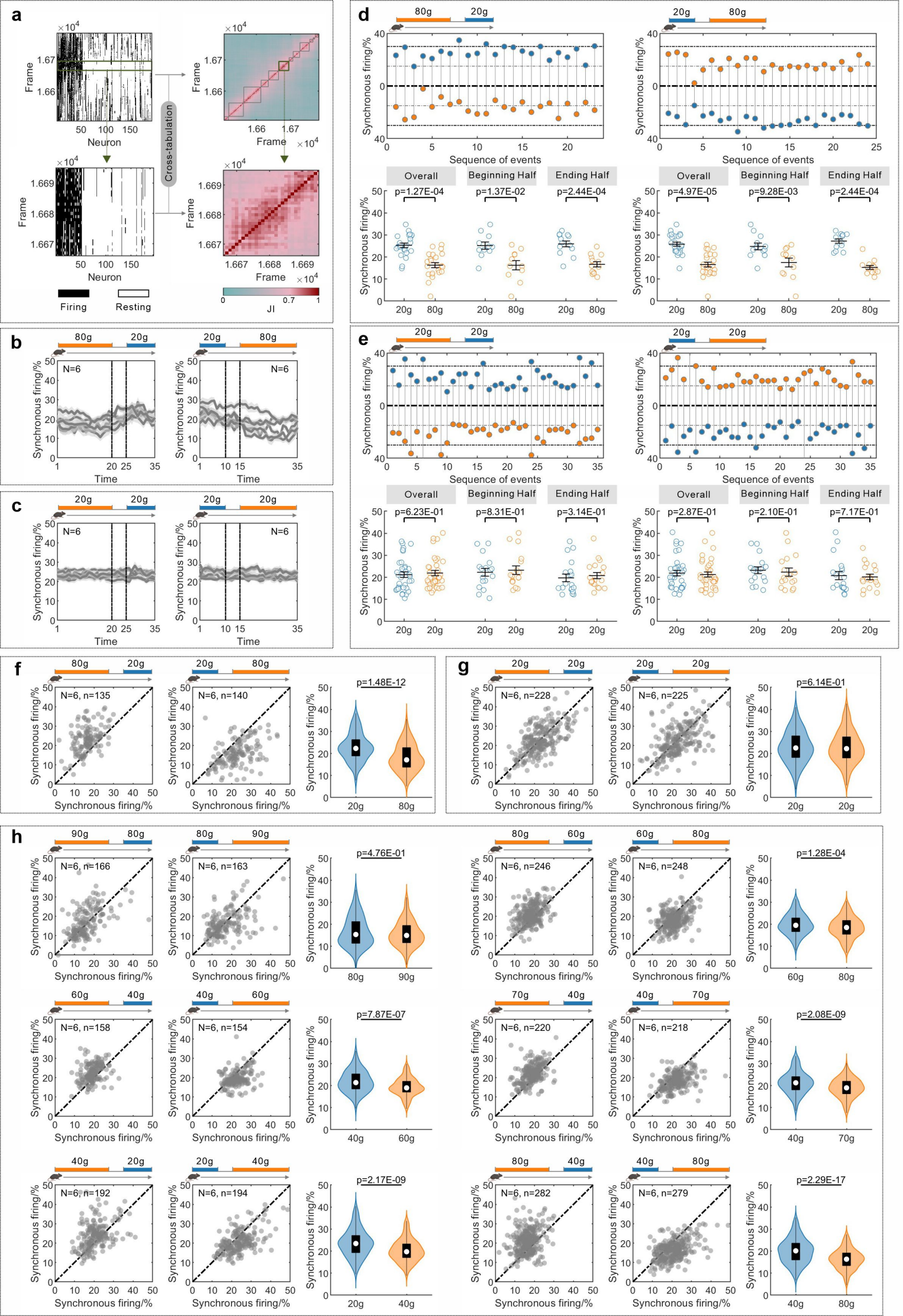
a
Frame
Neuron
Cross-tabulation
Firing
Resting
JI
b
c
d
e
f
g
h
80g
20g
90g
60g
40g
70g
Synchronous firing/%
Sequence of events
Time
Overall
Beginning Half
Ending Half
p=1.27E-04
p=1.37E-02
p=2.44E-04
p=4.97E-05
p=9.28E-03
p=2.44E-04
p=6.23E-01
p=8.31E-01
p=3.14E-01
p=2.87E-01
p=2.10E-01
p=7.17E-01
N=6
N=6, n=135
N=6, n=140
p=1.48E-12
N=6, n=228
N=6, n=225
p=6.14E-01
N=6, n=166
N=6, n=163
p=4.76E-01
N=6, n=246
N=6, n=248
p=1.28E-04
N=6, n=158
N=6, n=154
p=7.87E-07
N=6, n=220
N=6, n=218
p=2.08E-09
N=6, n=192
N=6, n=194
p=2.17E-09
N=6, n=282
N=6, n=279
p=2.29E-17

Fig. 3| Synchronous firing in the PPC neuronal population during quantity discrimination. a, The activation patterns of the PPC neuronal population at any given time (left), and the synchronous firing of a group of neurons (right, gray or green blocks), as indicated by the Jaccard Index (JI) calculation (Methods). **b**, **c**, Changes in the level of synchronous firing when the animal transitioned between foraging zones (**b**, 20g versus 80g; **c**, 20g versus 20g). Each line represents the mean ± s.e.m. trajectory for a mouse. **d**, **e**, The levels of synchronous firing in two typical mice during the quantity discrimination assay for 20g versus 80g of food (**d**), or 20g versus 20g of food (**e**) at either the beginning or the ending half. Two-tailed Wilcoxon signed-rank test; mean and s.e.m. are shown; dots manifest data from individual events. **f-h**, The levels of synchronous firing in the PPC neuronal population during quantity discrimination assay for 20g versus 80g of food (**f**), 20g versus 20g of food (**g**), or additional different amounts of food (**h**). Two-tailed Mann-Whitney U test; N indicates the number of mice; n indicates the number of events.

a

Shannon Entropy for Quantity Memory in Computer

A Transistor

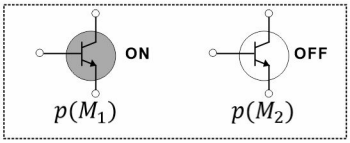

$$H(M) = \sum_{i=1}^{2} p(M_i) log_2^{1/p(M_i)}$$

A Byte of 8 Transistors

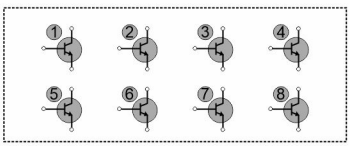

$$H = \sum_{M=1}^{8} \sum_{i=1}^{2} p(M_i) log_2^{1/p(M_i)}$$

A Population of Transistors

$$H = \sum_{M=1}^{S} \sum_{i=1}^{2} p(M_i) log_2^{1/p(M_i)}$$

S: The Number of Transistors in Population

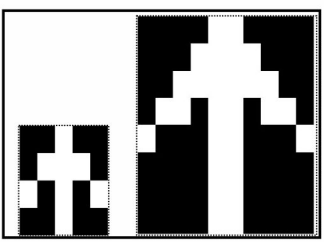

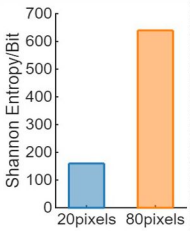

b

Neural Entropy for Quantity Discrimination in Brain

A Neuron

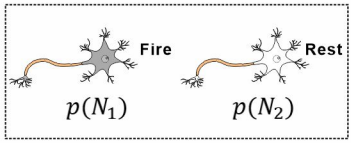

$$H(N) = \sum_{i=1}^{2} p(N_i) log_2^{1/p(N_i)}$$

A Pair of Neurons

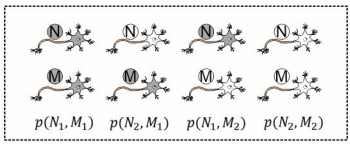

$$H(N, M) = \sum_{j=1}^{2} \sum_{i=1}^{2} p(N_j, M_i) log_2^{1/p(N_j, M_i)}$$

A Population of Neurons

$$N(X) = \frac{p(X)}{C_S^2} \sum_{N=1}^{S-1} \sum_{M=N+1}^{S} H(N, M)$$

S: The Number of Neurons in Population
p(X): Probability at Condition X
C_S^2: Pairs of Synchronous Firing Neurons

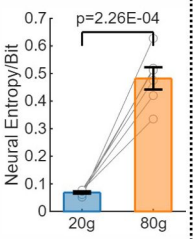

Fig. 4| Neural Entropy model for quantity discrimination. a, Calculation of Shannon Entropy for a single memory transistor, a Byte of eight transistors, and a population of transistors on a chip. The specified entropy values for encoding images with either 20 or 80 pixels. **b**, Calculation of Information content for a single neuron, a pair of neurons, and a population of neurons in the PPC. The Neural Entropy values for synchronous firing are calculated from the neuronal activity of the PPC during quantity discrimination for 20g versus 80g of food. Two-tailed paired t-test; mean and s.e.m. are shown; dots manifest data from individual mice (N=6).

352 **Table 1. Levels of synchronous firing during quantity discrimination**

Amounts of Food (g/g)	Levels of Synchronous Firing (%) [a]	Statistical Significance (p-value) [b]
20:20	23.34±0.55:23.51±0.66	6.14E-01
80:90	17.20±0.84:15.91±0.57	4.76E-01
60:80	21.02±0.28:18.27±0.52	1.28E-04
40:60	22.49±0.29:19.25±0.30	7.87E-07
40:70	22.25±0.36:18.61±0.18	2.08E-09
20:40	24.02±0.83:20.81±0.95	2.17E-09
40:80	21.28±0.35:16.40±0.38	2.29E-17
20:80	23.33±0.76:16.61±0.75	1.48E-12

353 [a] Values are presented as mean ± s.e.m. (N=6).

354 [b] Two-tailed Mann-Whitney U test.

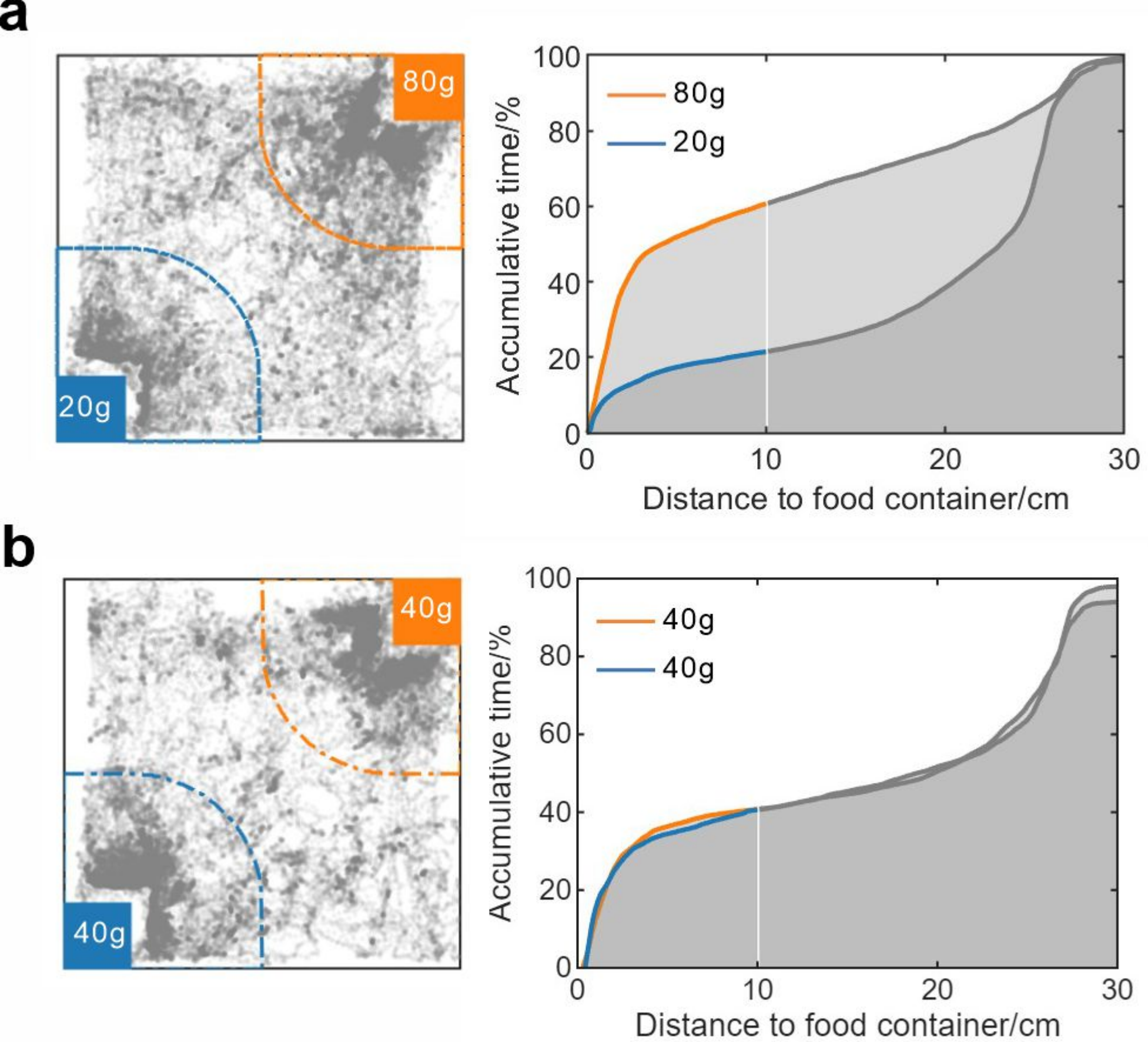
a
80g
20g
100
80
60
40
20
0
Accumulative time/%
80g
20g
0
10
20
30
Distance to food container/cm
b
40g
40g
100
80
60
40
20
0
Accumulative time/%
40g
40g
0
10
20
30
Distance to food container/cm

Extended Data Fig. 1| Tracking map in the food quantity discrimination assay. a, b, Representative tracking map illustrating the percentage of time the mouse spent in each foraging zone (**a**, 20g versus 80g; **b**, 40g versus 40g), along with its proximity to the food containers.

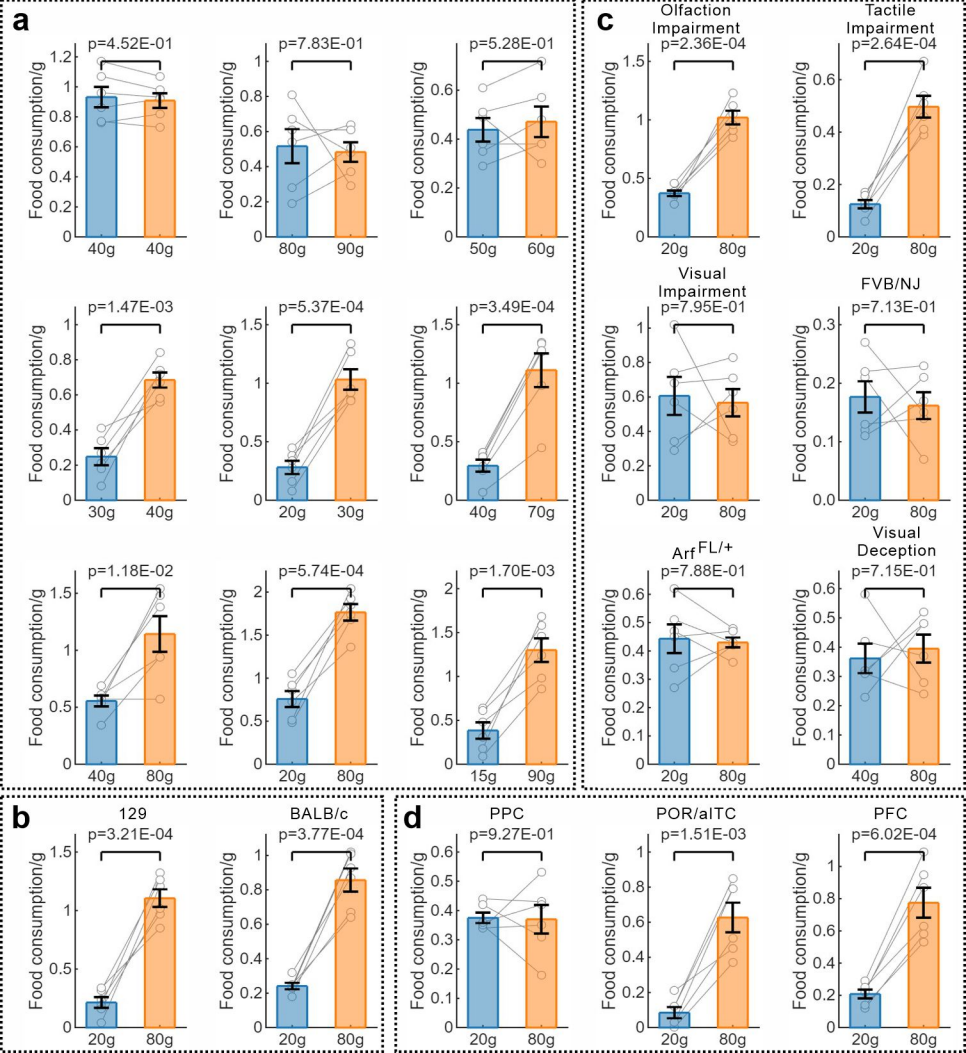
a
p=4.52E-01
40g
40g
p=7.83E-01
80g
90g
p=5.28E-01
50g
60g
p=1.47E-03
30g
40g
p=5.37E-04
20g
30g
p=3.49E-04
40g
70g
p=1.18E-02
40g
80g
p=5.74E-04
20g
80g
p=1.70E-03
15g
90g
c
Olfaction Impairment
p=2.36E-04
20g
80g
Tactile Impairment
p=2.64E-04
20g
80g
Visual Impairment
p=7.95E-01
20g
80g
FVB/NJ
p=7.13E-01
20g
80g
Arf FL/+
p=7.88E-01
20g
80g
Visual Deception
p=7.15E-01
40g
80g
b
129
p=3.21E-04
20g
80g
BALB/c
p=3.77E-04
20g
80g
d
PPC
p=9.27E-01
20g
80g
POR/aITC
p=1.51E-03
20g
80g
PFC
p=6.02E-04
20g
80g
Food consumption/g

Extended Data Fig. 2| Food consumption in the food quantity discrimination assay. **a**, Food consumption by C57BL/6J mice in different quantity discrimination assays. **b**, Food consumption by 129 and BALB/c mice. **c**, Food consumption by individual mice in sensory input deprivation experiments. **d**, Food consumption by C57BL/6J mice in the experiments of inhibition of the PPC, the POR/aITC, or the PFC. For **a-d**, Two-tailed paired t-test; mean and s.e.m. are shown; dots manifest data from individual mice (N=6).

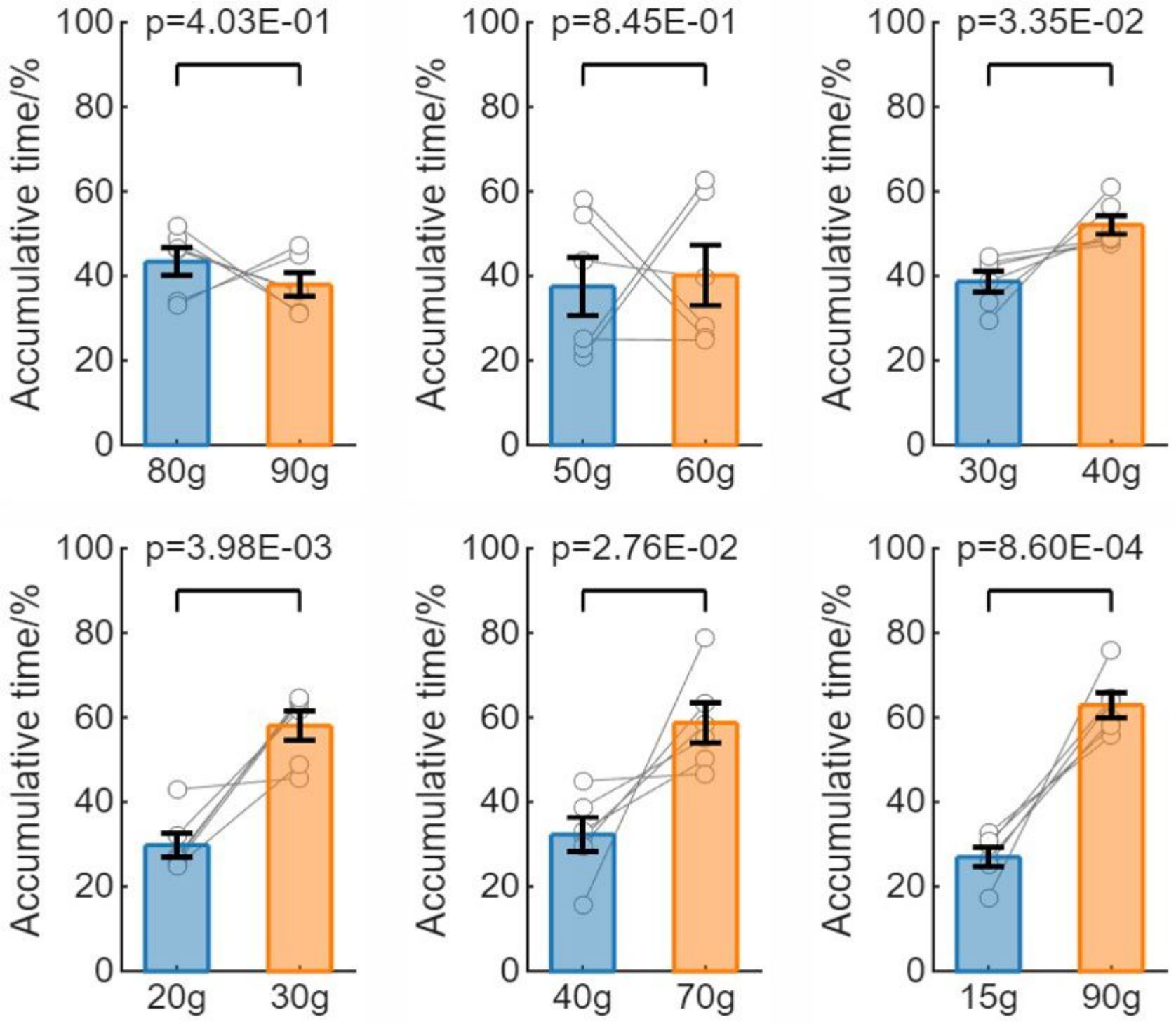
p=4.03E-01
Accumulative time/%
100
80
60
40
20
0
80g
90g
p=8.45E-01
Accumulative time/%
100
80
60
40
20
0
50g
60g
p=3.35E-02
Accumulative time/%
100
80
60
40
20
0
30g
40g
p=3.98E-03
Accumulative time/%
100
80
60
40
20
0
20g
30g
p=2.76E-02
Accumulative time/%
100
80
60
40
20
0
40g
70g
p=8.60E-04
Accumulative time/%
100
80
60
40
20
0
15g
90g

Extended Data Fig. 3| Quantity discrimination for additional food amounts in mice. Quantity discrimination behavior for different ratios of food amounts in the C57BL/6J. Two-tailed paired t-test; mean and s.e.m. are shown; dots manifest data from individual mice (N=6).

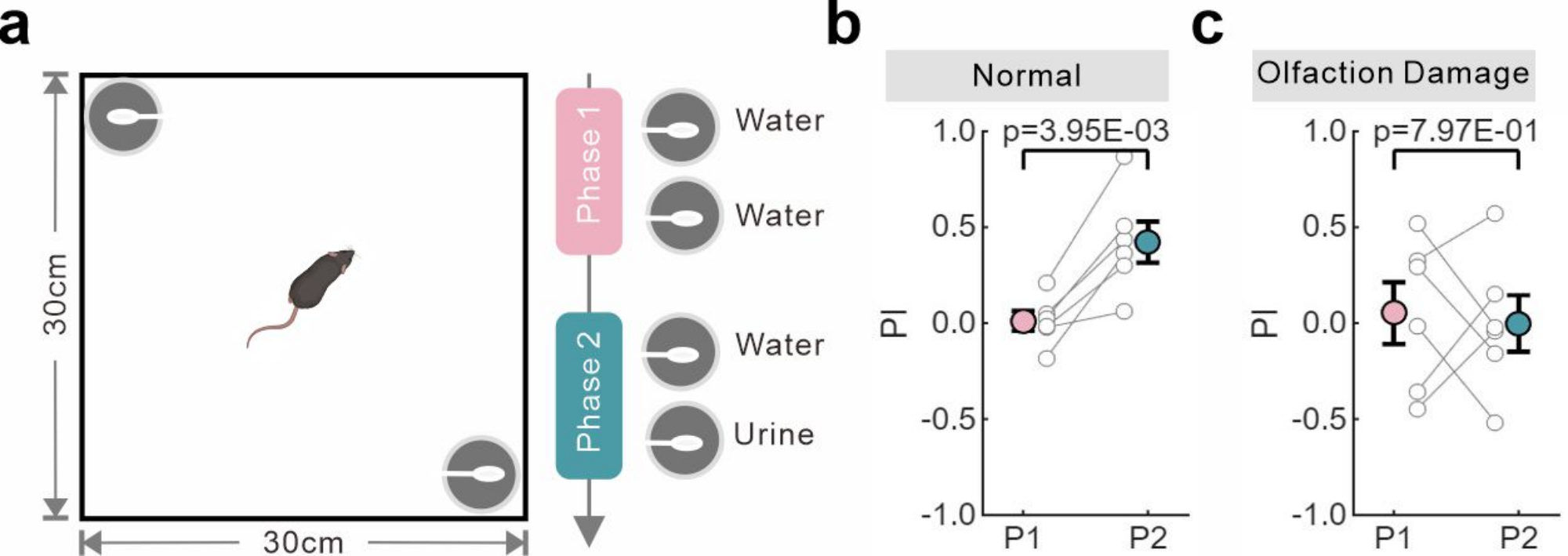
a
30cm
30cm
Phase 1
Phase 2
Water
Water
Water
Urine
b
Normal
p=3.95E-03
1.0
0.5
0.0
-0.5
-1.0
PI
P1
P2
c
Olfaction Damage
p=7.97E-01
1.0
0.5
0.0
-0.5
-1.0
PI
P1
P2

Extended Data Fig. 4| Olfactory test. a, The exhibition of various olfactory cues in an open arena (Methods). **b, c**, Preference Index (PI) values for olfactory cues during different experimental phases under normal condition (**b**) or following induced deprivation of olfactory sensation (**c**). Two-tailed paired t-test; mean and s.e.m. are shown; dots manifest data from individual mice (N=6).

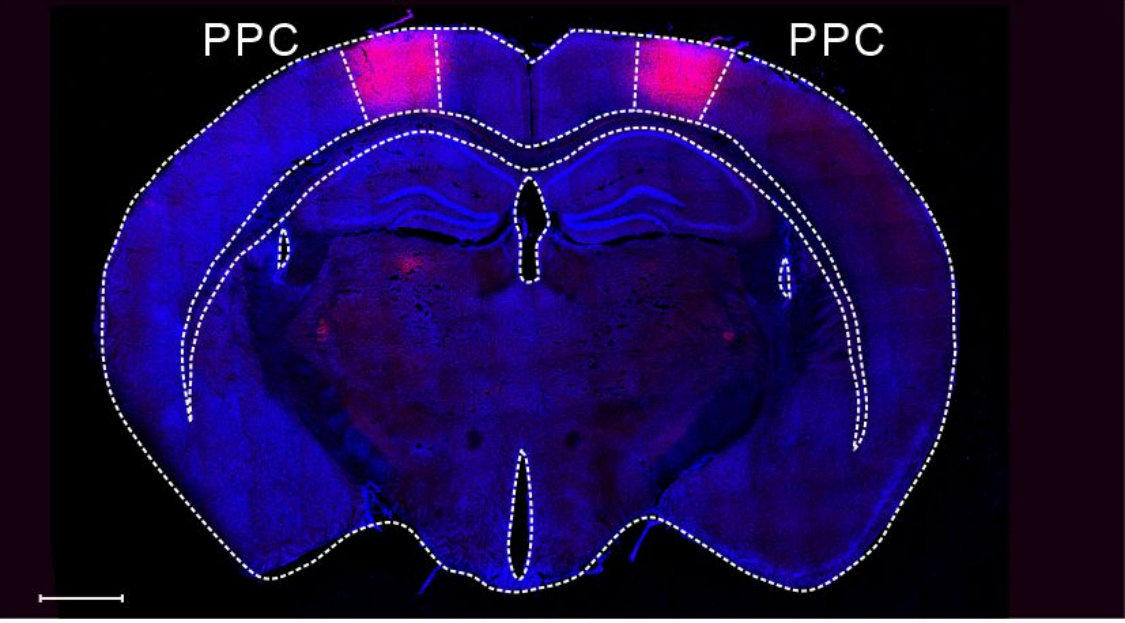
PPC
PPC

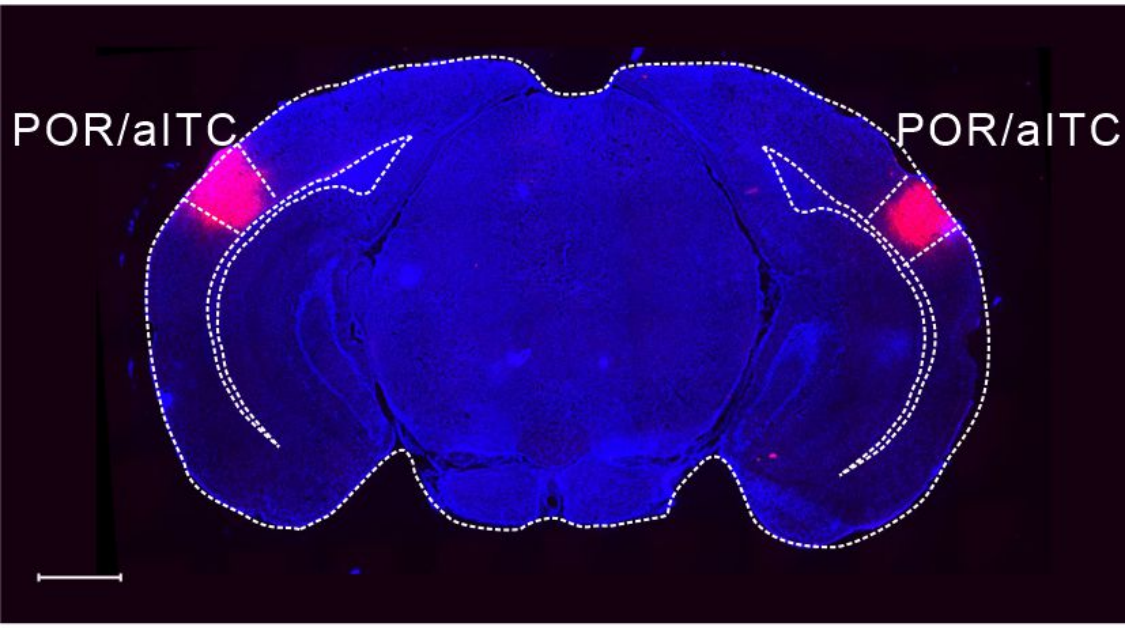
POR/alTC
POR/alTC

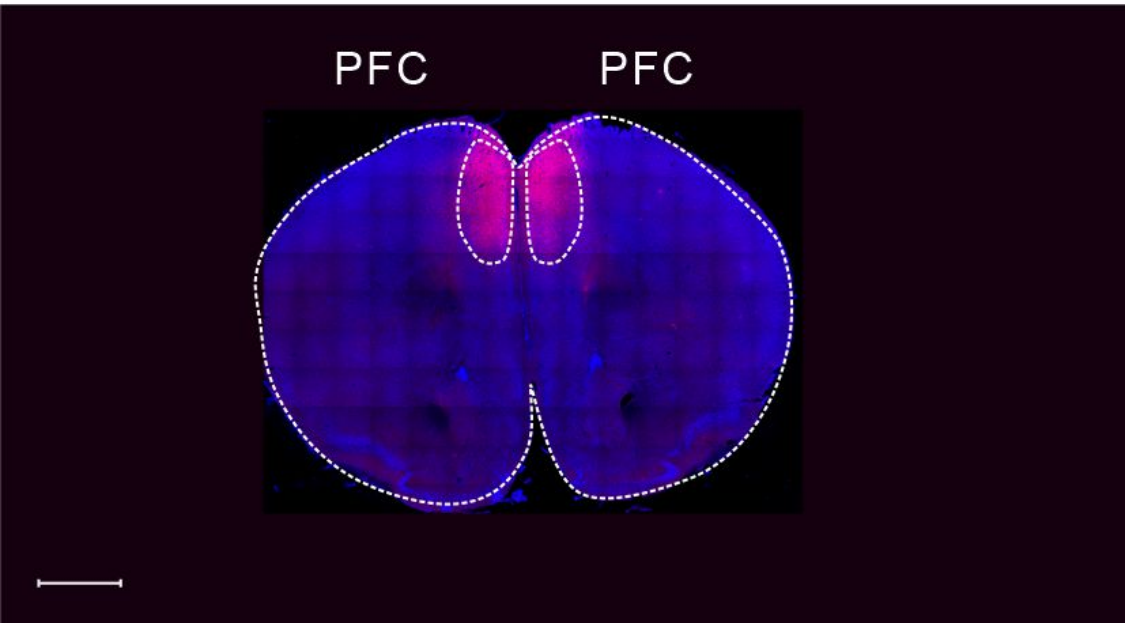
PFC
PFC

Extended Data Fig. 5| Inhibition of different cortex regions. Site-specific delivery of a viral vector expressing an inhibitory channel, AAV9-hSyn-hM4Di-mCherry, was performed in different cortex regions: the PPC (top), the POR/aITC (middle), or the PFC (bottom), as described in the Methods. Scale bars: 1mm.

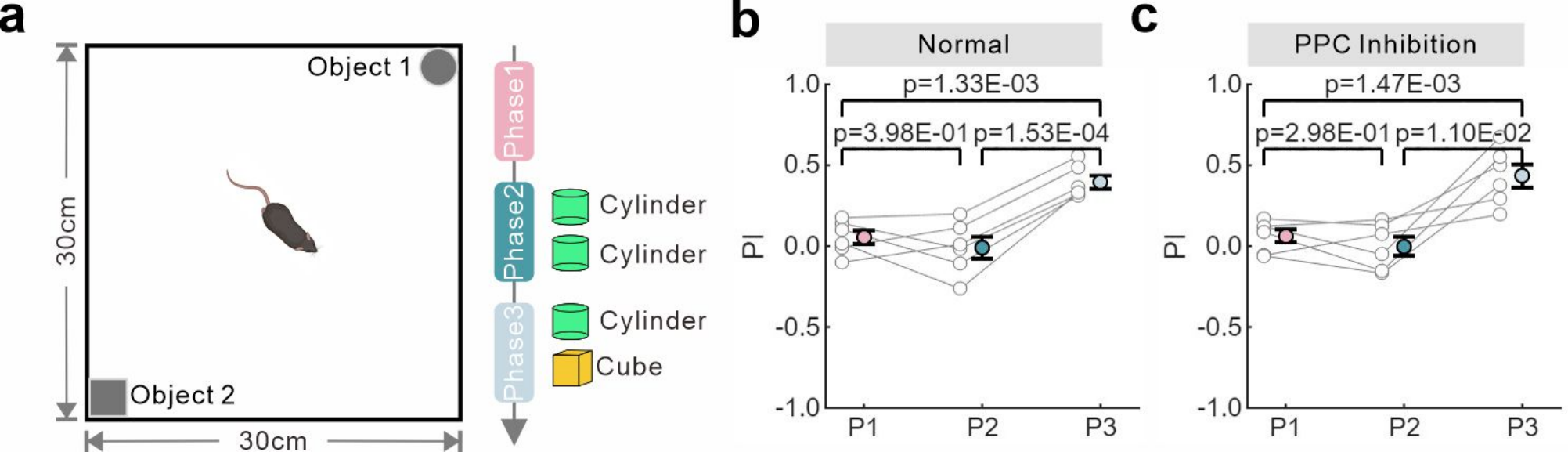
a
Object 1
Object 2
30cm
30cm
Phase1
Phase2
Phase3
Cylinder
Cylinder
Cylinder
Cube
b
Normal
p=1.33E-03
p=3.98E-01
p=1.53E-04
PI
1.0
0.5
0.0
-0.5
-1.0
P1
P2
P3
c
PPC Inhibition
p=1.47E-03
p=2.98E-01
p=1.10E-02
PI
1.0
0.5
0.0
-0.5
-1.0
P1
P2
P3

Extended Data Fig. 6| Novel object recognition test. a, The positions of different objects in an open arena (Methods). **b, c**, Preference Index (PI) values for objects during different experimental phases under normal condition (**b**) or following inhibition of neuronal activity in the PPC (**c**). Two-tailed paired t-test; mean and s.e.m. are shown; dots manifest data from individual mice (N=6).

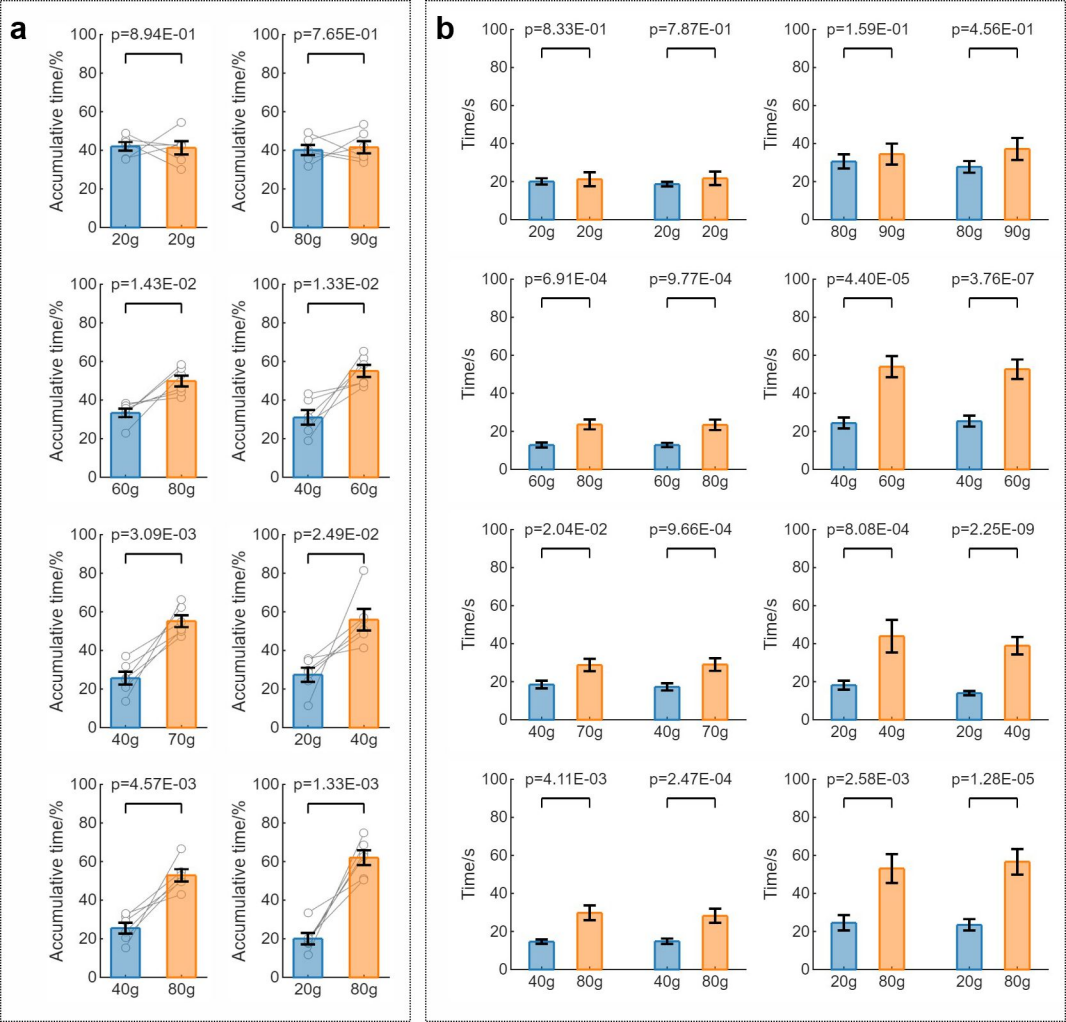
a
Accumulative time/%
p=8.94E-01
20g
20g
p=7.65E-01
80g
90g
p=1.43E-02
60g
80g
p=1.33E-02
40g
60g
p=3.09E-03
40g
70g
p=2.49E-02
20g
40g
p=4.57E-03
40g
80g
p=1.33E-03
20g
80g
b
Time/s
p=8.33E-01
20g
20g
p=7.87E-01
20g
20g
p=1.59E-01
80g
90g
p=4.56E-01
80g
90g
p=6.91E-04
60g
80g
p=9.77E-04
60g
80g
p=4.40E-05
40g
60g
p=3.76E-07
40g
60g
p=2.04E-02
40g
70g
p=9.66E-04
40g
70g
p=8.08E-04
20g
40g
p=2.25E-09
20g
40g
p=4.11E-03
40g
80g
p=2.47E-04
40g
80g
p=2.58E-03
20g
80g
p=1.28E-05
20g
80g

Extended Data Fig. 7| Quantity discrimination behavior during two-photon imaging experiments. a, Quantity discrimination behavior for different amounts of food during the two-photon imaging experiments. Two-tailed Paired t-test; mean and s.e.m. are shown; dots manifest data from individual mice (N=6). **b**, Time allocation in foraging zones during zone transitions when different amounts of food were presented. for given amounts of food (*e.g.*, 20g versus 80g), left panels show transitions from more-amount to less-amount foraging zones, while right panels show the reverse transition pattern. Two-tailed Wilcoxon signed-rank test; mean and s.e.m. are shown.

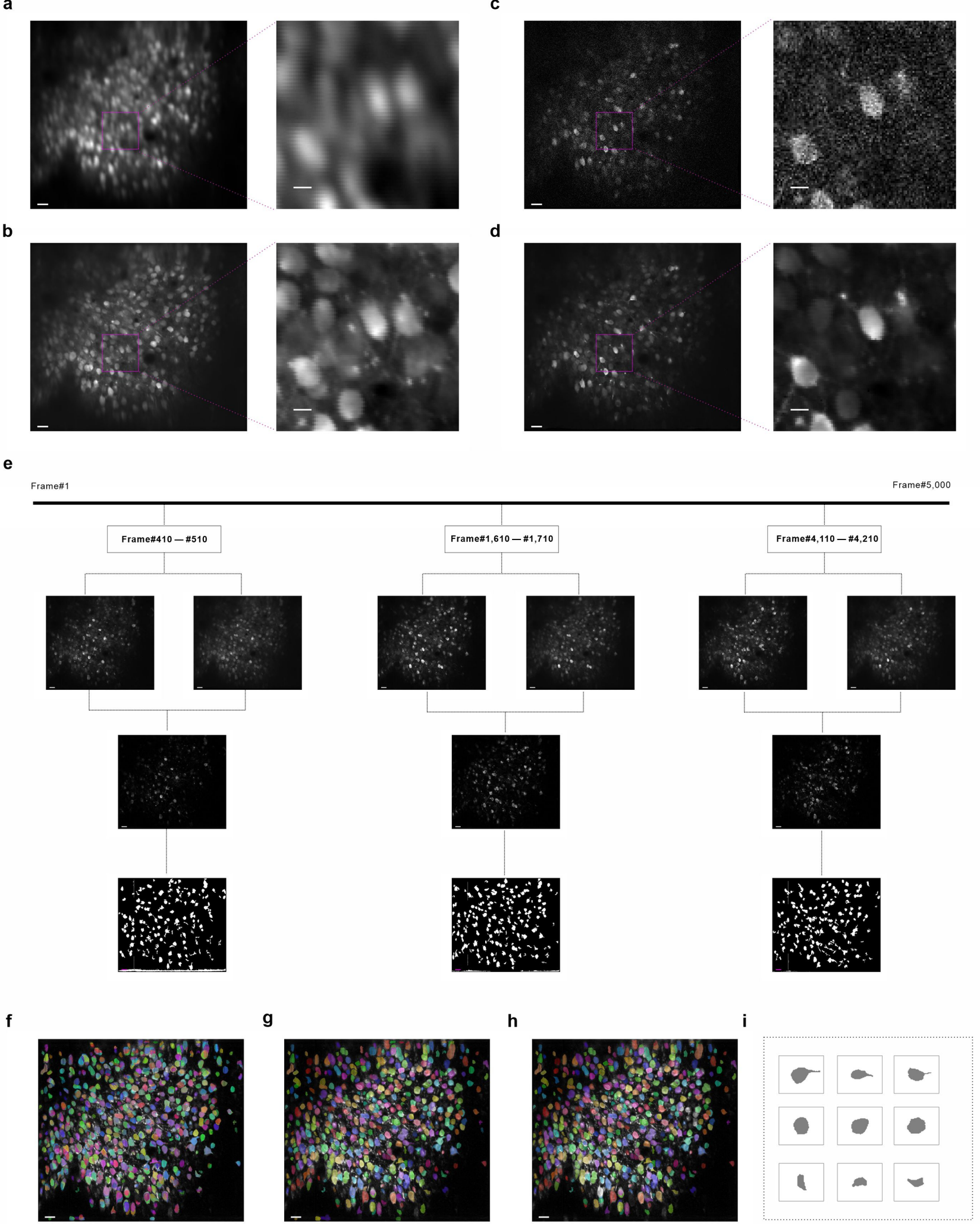
a
c
b
d
e
Frame#1
Frame#5,000
Frame#410 — #510
Frame#1,610 — #1,710
Frame#4,110 — #4,210
f
g
h
i

Extended Data Fig. 8| Two-photon imaging data processing. a, b, Mean projection images of all frames before (**a**) and after (**b**) applying motion correction. **c, d**, A single frame before (**c**) and after (**d**) noise reduction. **e**, Three representative periodic blocks, each consisting of 100 consecutive frames. For each block, the maximum projection image (upper left), mean projection image (upper right), max-mean projection image (middle), and corresponding periodic mask (lower) are displayed. **f-h**, Illustrations of the temporal mask (**f**), spatial mask (**g**), and soma mask (**h**). **i**, Examples of typical soma. Scale bars: 30 pixels (**e**, left panels in **a-d**, **f-h**) or 10 pixels (right panels in **a-d**).

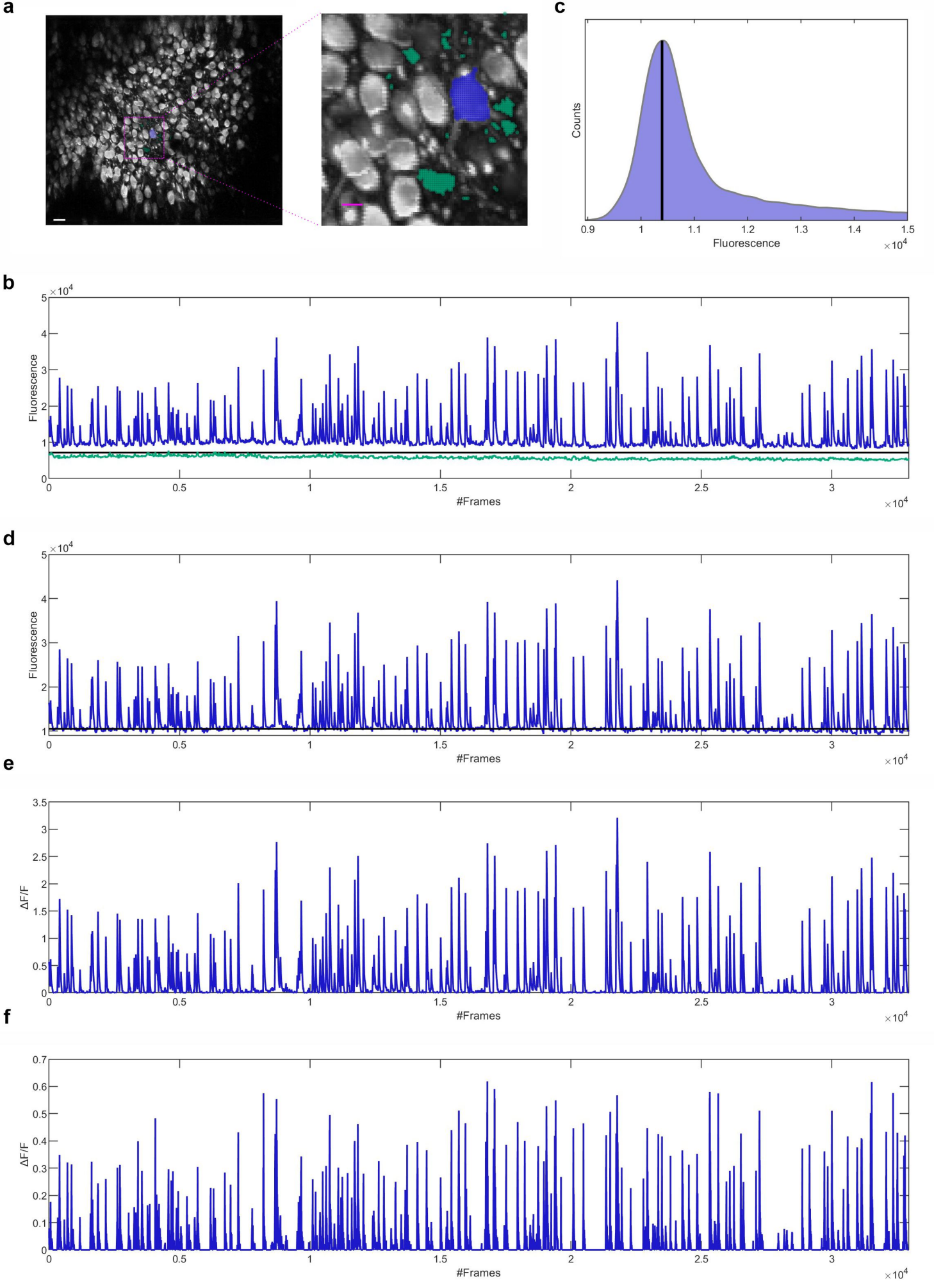
a
c
Counts
Fluorescence
×10^4
b
Fluorescence
#Frames
×10^4
d
Fluorescence
#Frames
×10^4
e
ΔF/F
#Frames
×10^4
f
ΔF/F
#Frames
×10^4

Extended Data Fig. 9| Extraction of neuronal activity signals. a, A typical neuron (blue) and its corresponding neuropil (green). Scale bars: 30 pixels (left) or 10 pixels (right). **b**, The average fluorescence intensity recorded from the neuron (blue) and its neuropil (green) throughout the entire recording session. The black line indicates the 3σ level of the background fluorescence. **c**, Distribution of average fluorescence intensity across individual frames along with the baseline (black line). **d**, The fluorescence trace of the neuron after correction for neuropil contamination and detrending to remove polynomial trends. The black line represents the baseline fluorescence. **e**, The calcium signal of the neuron. **f**, The event signal of the neuron.

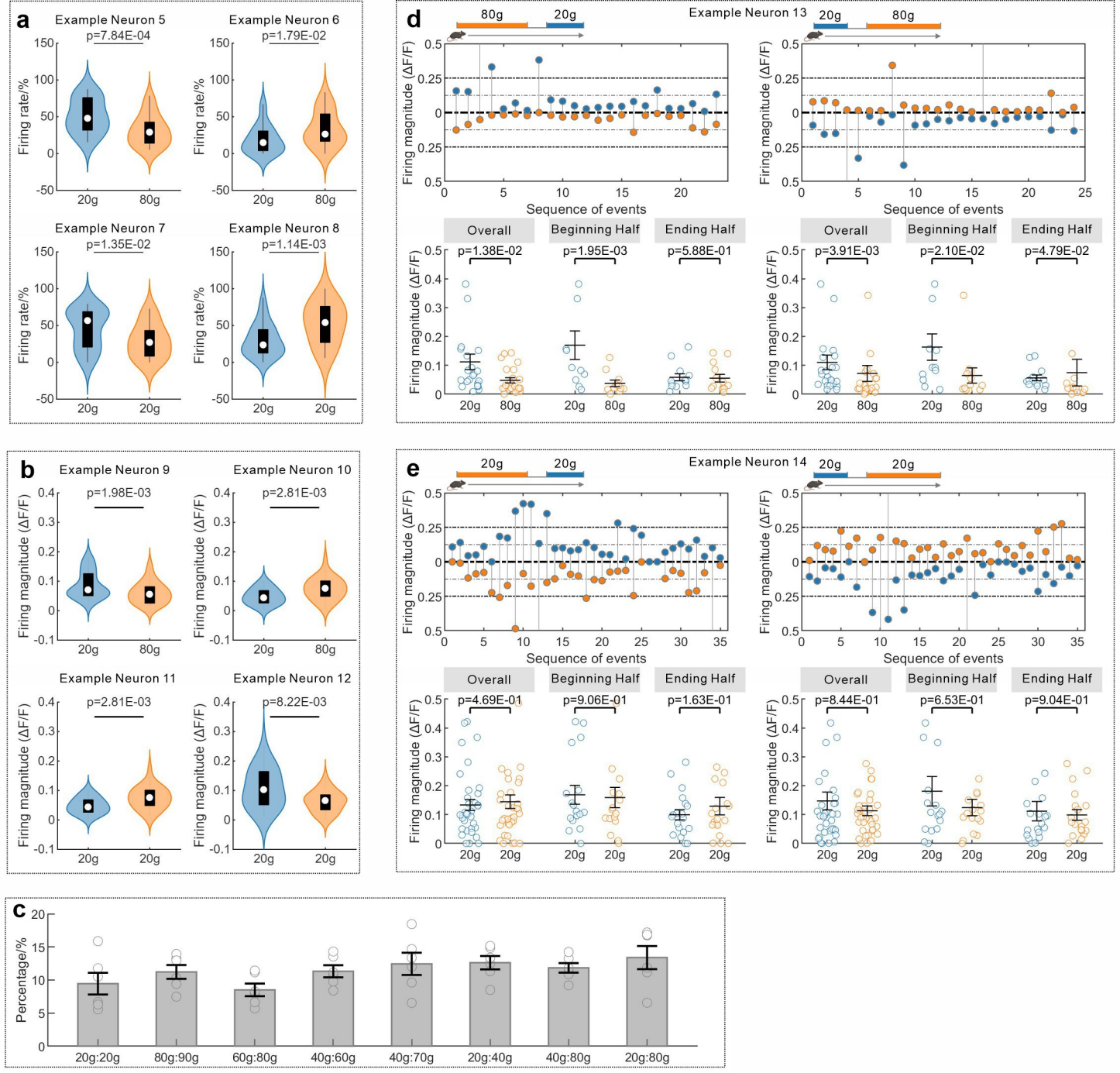
a
Example Neuron 5
p=7.84E-04
Example Neuron 6
p=1.79E-02
Example Neuron 7
p=1.35E-02
Example Neuron 8
p=1.14E-03
Firing rate/%
20g
80g
b
Example Neuron 9
p=1.98E-03
Example Neuron 10
p=2.81E-03
Example Neuron 11
p=2.81E-03
Example Neuron 12
p=8.22E-03
Firing magnitude (ΔF/F)
c
Percentage/%
20g:20g
80g:90g
60g:80g
40g:60g
40g:70g
20g:40g
40g:80g
20g:80g
d
Example Neuron 13
80g
20g
Firing magnitude (ΔF/F)
Sequence of events
Overall
Beginning Half
Ending Half
p=1.38E-02
p=1.95E-03
p=5.88E-01
p=3.91E-03
p=2.10E-02
p=4.79E-02
e
Example Neuron 14
20g
p=4.69E-01
p=9.06E-01
p=1.63E-01
p=8.44E-01
p=6.53E-01
p=9.04E-01

Extended Data Fig. 10| Neurons with preferential activities at a given time. a, b, Typical neurons with preferential activities towards a specific amount of food, evaluated by comparing their firing rate (**a**) or firing magnitude (**b**) across different foraging zones. Two-tailed Mann-Whitney U test. **c**, The percentage of neurons showing preferential activities for specific amounts of food. mean and s.e.m. are shown; dots manifest data from individual mice. **d, e**, Preferential activities of two typical neurons in the PPC during the quantity discrimination assay for 20g versus 80g of food (**d**), or 20g versus 20g of food (**e**) at either the beginning or the ending half. Two-tailed Wilcoxon signed-rank test; mean and s.e.m. are shown; dots manifest data from individual events.

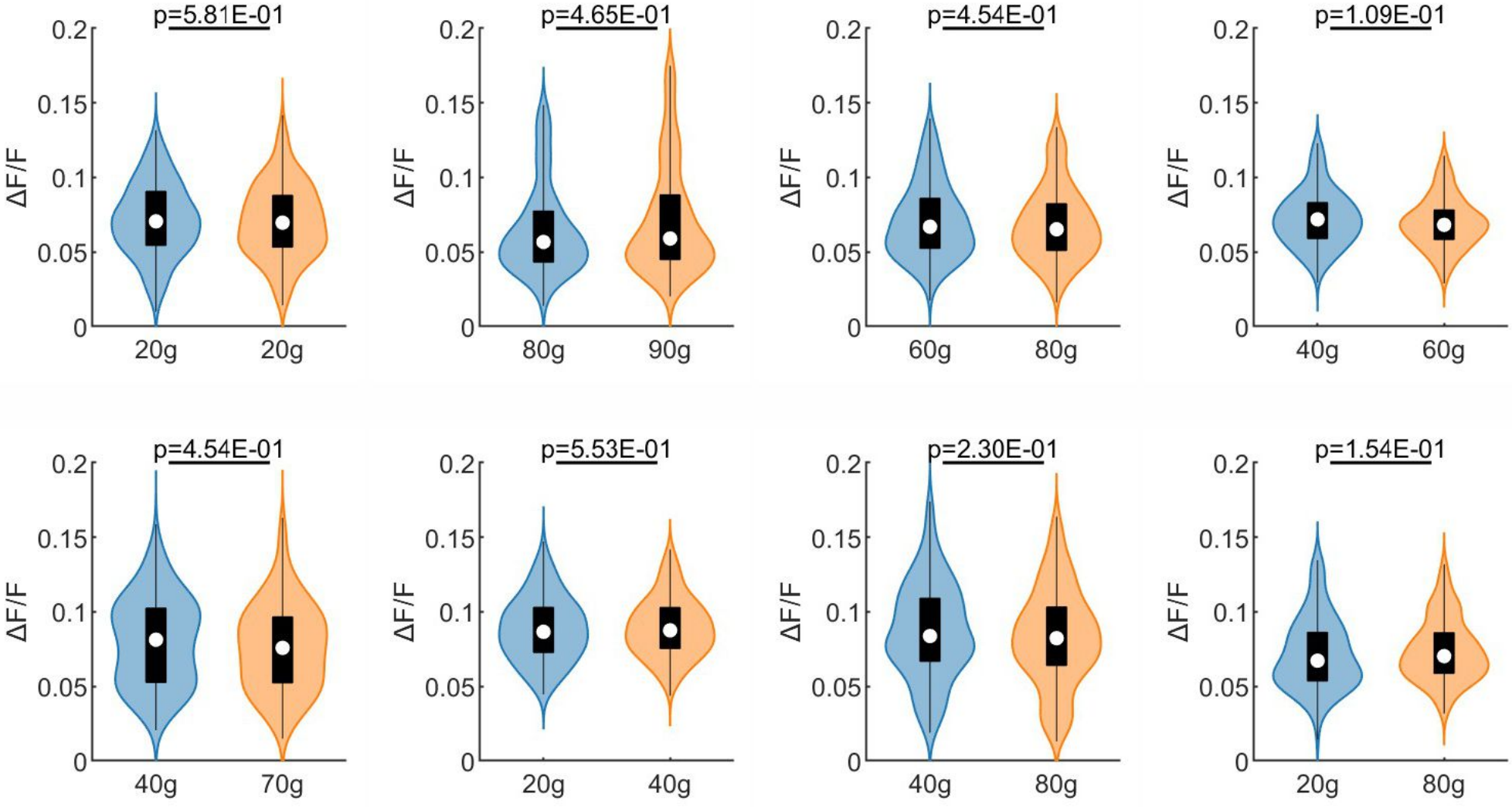
p=5.81E-01
p=4.65E-01
p=4.54E-01
p=1.09E-01
p=4.54E-01
p=5.53E-01
p=2.30E-01
p=1.54E-01
ΔF/F
0
0.05
0.1
0.15
0.2
20g
20g
80g
90g
60g
80g
40g
60g
40g
70g
20g
40g
40g
80g
20g
80g

Extended Data Fig. 11| Firing magnitude of the PPC neuronal population. The firing magnitude of the PPC neuronal population when the animals were presented with different amounts of food. Two-tailed Mann-Whitney U test.

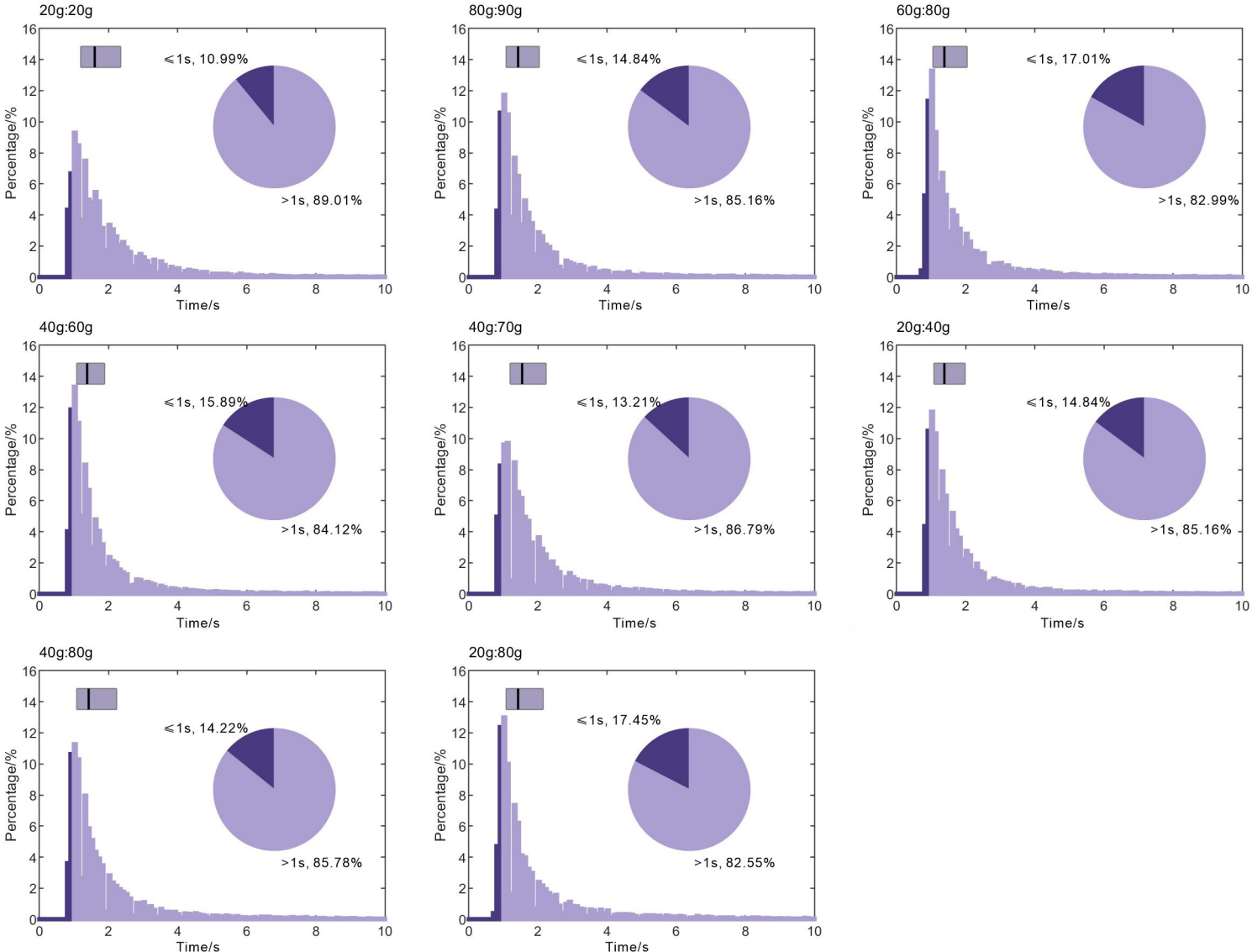
20g:20g
≤1s, 10.99%
>1s, 89.01%
80g:90g
≤1s, 14.84%
>1s, 85.16%
60g:80g
≤1s, 17.01%
>1s, 82.99%
40g:60g
≤1s, 15.89%
>1s, 84.12%
40g:70g
≤1s, 13.21%
>1s, 86.79%
20g:40g
≤1s, 14.84%
>1s, 85.16%
40g:80g
≤1s, 14.22%
>1s, 85.78%
20g:80g
≤1s, 17.45%
>1s, 82.55%
Percentage/%
Time/s

Extended Data Fig.12| Duration of synchronous firing. The duration of synchronous firing in the PPC neuronal population, illustrated with a pie chart depicting the proportion of patterns classified using a 1-second threshold.

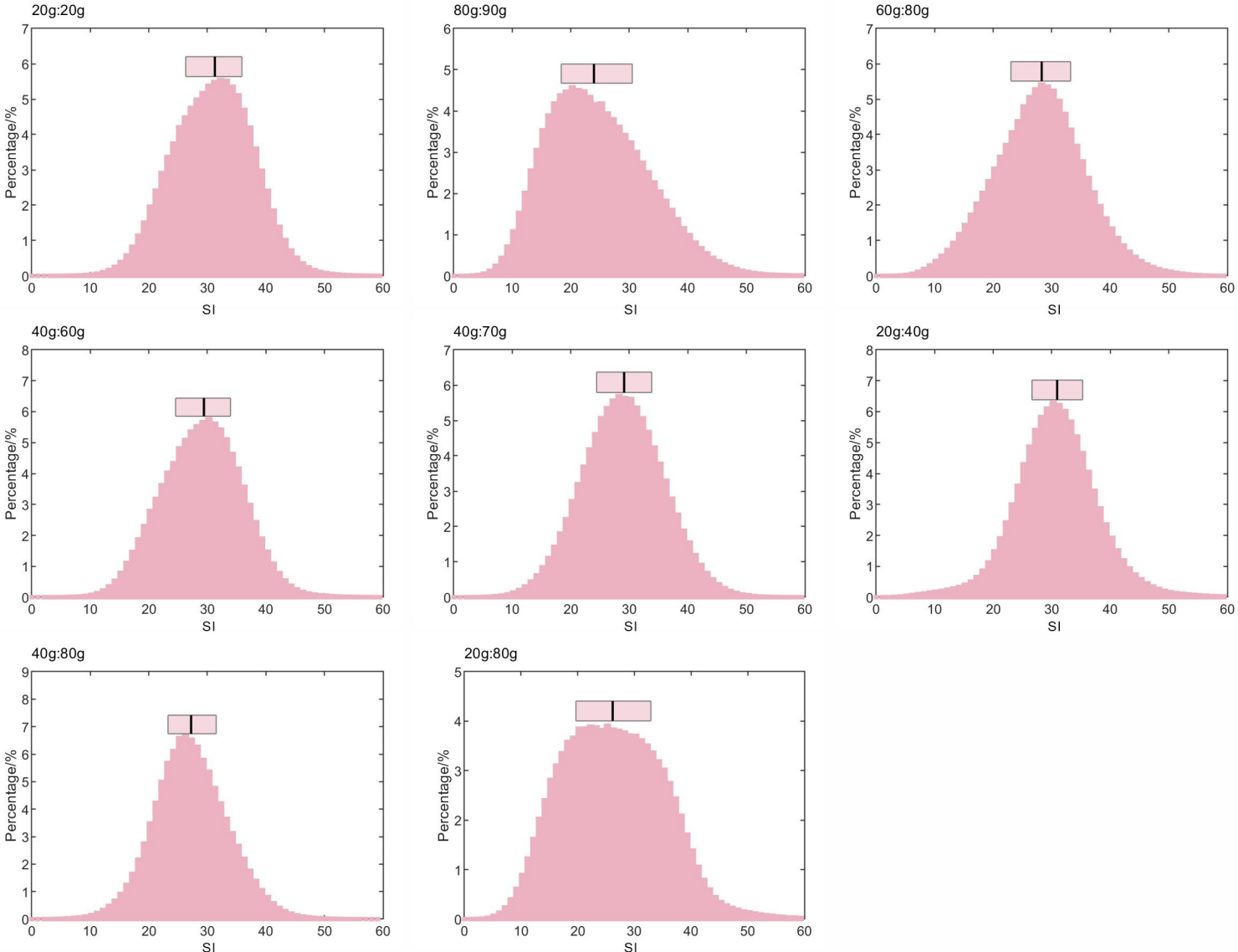
20g:20g
80g:90g
60g:80g
40g:60g
40g:70g
20g:40g
40g:80g
20g:80g
Percentage/%
SI

Extended Data Fig. 13| Distribution of similarity index. The distribution of similarity index (SI) between any pair of synchronous firings (Methods).

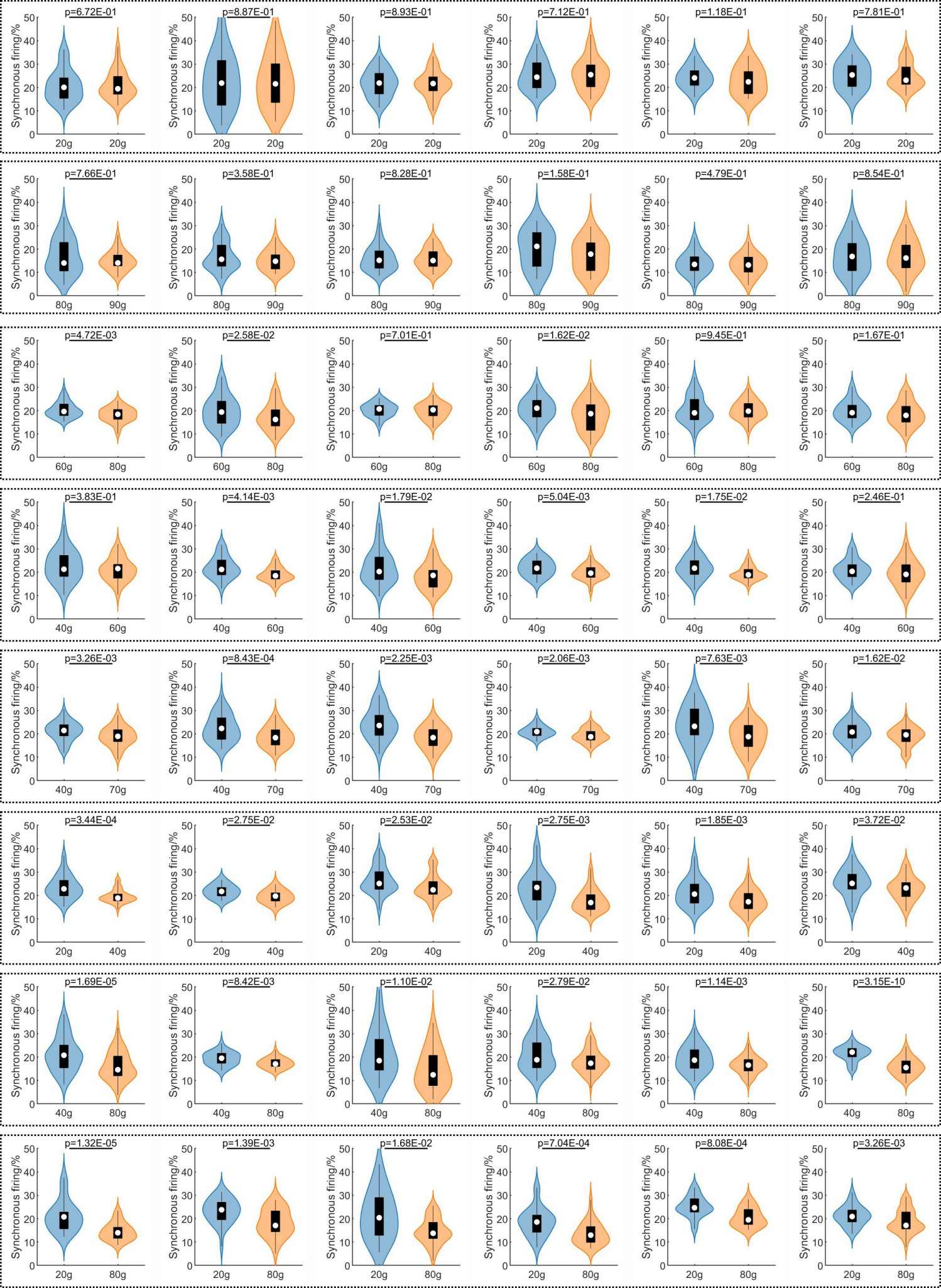
p=6.72E-01
p=8.87E-01
p=8.93E-01
p=7.12E-01
p=1.18E-01
p=7.81E-01
20g 20g
p=7.66E-01
p=3.58E-01
p=8.28E-01
p=1.58E-01
p=4.79E-01
p=8.54E-01
80g 90g
p=4.72E-03
p=2.58E-02
p=7.01E-01
p=1.62E-02
p=9.45E-01
p=1.67E-01
60g 80g
p=3.83E-01
p=4.14E-03
p=1.79E-02
p=5.04E-03
p=1.75E-02
p=2.46E-01
40g 60g
p=3.26E-03
p=8.43E-04
p=2.25E-03
p=2.06E-03
p=7.63E-03
p=1.62E-02
40g 70g
p=3.44E-04
p=2.75E-02
p=2.53E-02
p=2.75E-03
p=1.85E-03
p=3.72E-02
20g 40g
p=1.69E-05
p=8.42E-03
p=1.10E-02
p=2.79E-02
p=1.14E-03
p=3.15E-10
40g 80g
p=1.32E-05
p=1.39E-03
p=1.68E-02
p=7.04E-04
p=8.08E-04
p=3.26E-03
20g 80g
Synchronous firing/%
0 10 20 30 40 50

Extended Data Fig. 14| The levels of synchronous firing. The levels of synchronous firing in the PPC neuronal population when individual mice were presented with different food amounts. Two-tailed Mann-Whitney U test.

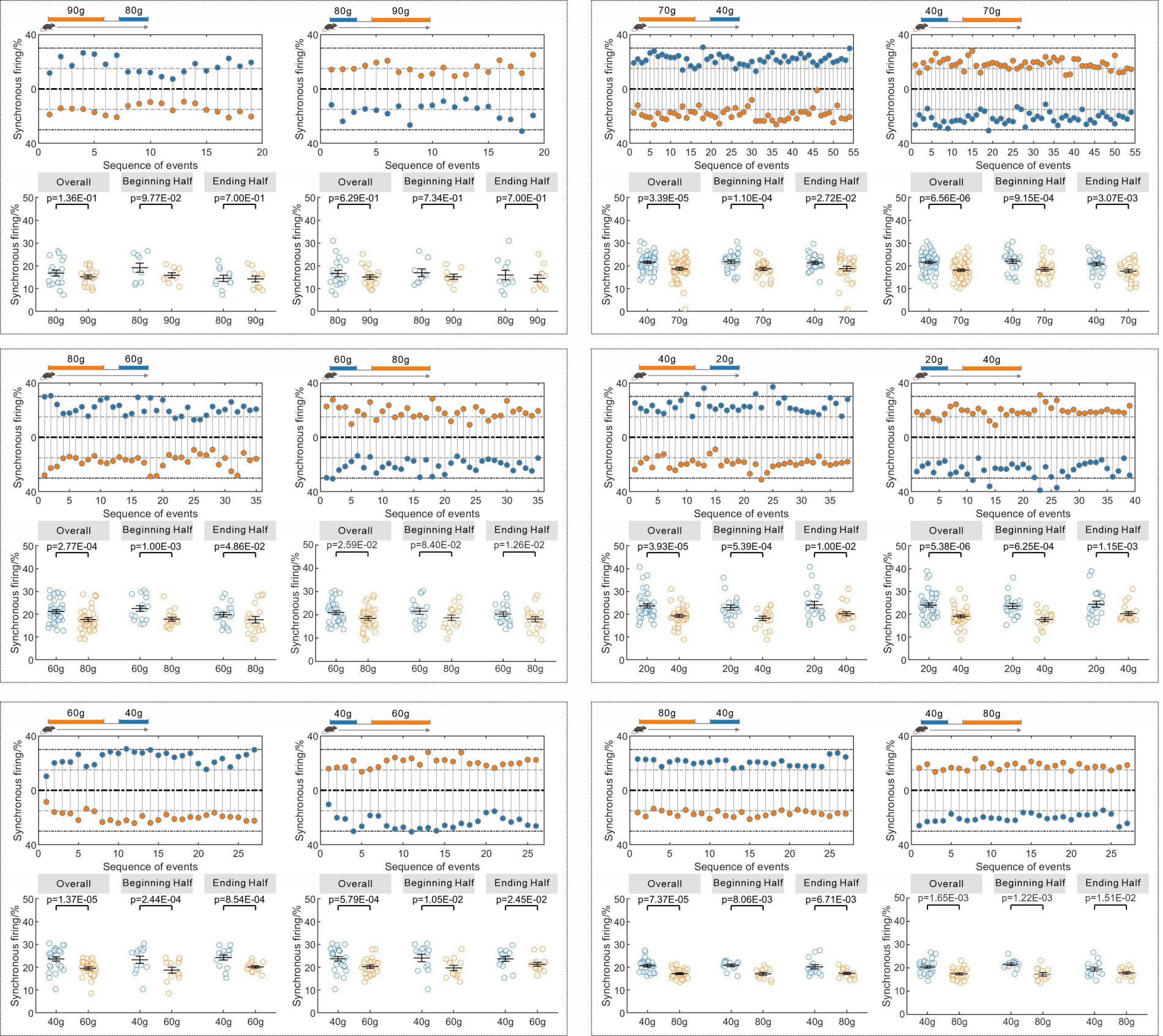
90g 80g
80g 90g
70g 40g
40g 70g
80g 60g
60g 80g
40g 20g
20g 40g
60g 40g
40g 60g
80g 40g
40g 80g
Synchronous firing/%
Sequence of events
Overall
Beginning Half
Ending Half
p=1.36E-01 p=9.77E-02 p=7.00E-01
p=6.29E-01 p=7.34E-01 p=7.00E-01
p=3.39E-05 p=1.10E-04 p=2.72E-02
p=6.56E-06 p=9.15E-04 p=3.07E-03
p=2.77E-04 p=1.00E-03 p=4.86E-02
p=2.59E-02 p=8.40E-02 p=1.26E-02
p=3.93E-05 p=5.39E-04 p=1.00E-02
p=5.38E-06 p=6.25E-04 p=1.15E-03
p=1.37E-05 p=2.44E-04 p=8.54E-04
p=5.79E-04 p=1.05E-02 p=2.45E-02
p=7.37E-05 p=8.06E-03 p=6.71E-03
p=1.65E-03 p=1.22E-03 p=1.51E-02

Extended Data Fig. 15| Changes in the levels of synchronous firing during quantity discrimination. The levels of synchronous firing in typical mice during the quantity discrimination assay for different amounts of food at either the beginning or the ending half. Two-tailed Wilcoxon signed-rank test; mean and s.e.m. are shown; dots manifest data from individual events.

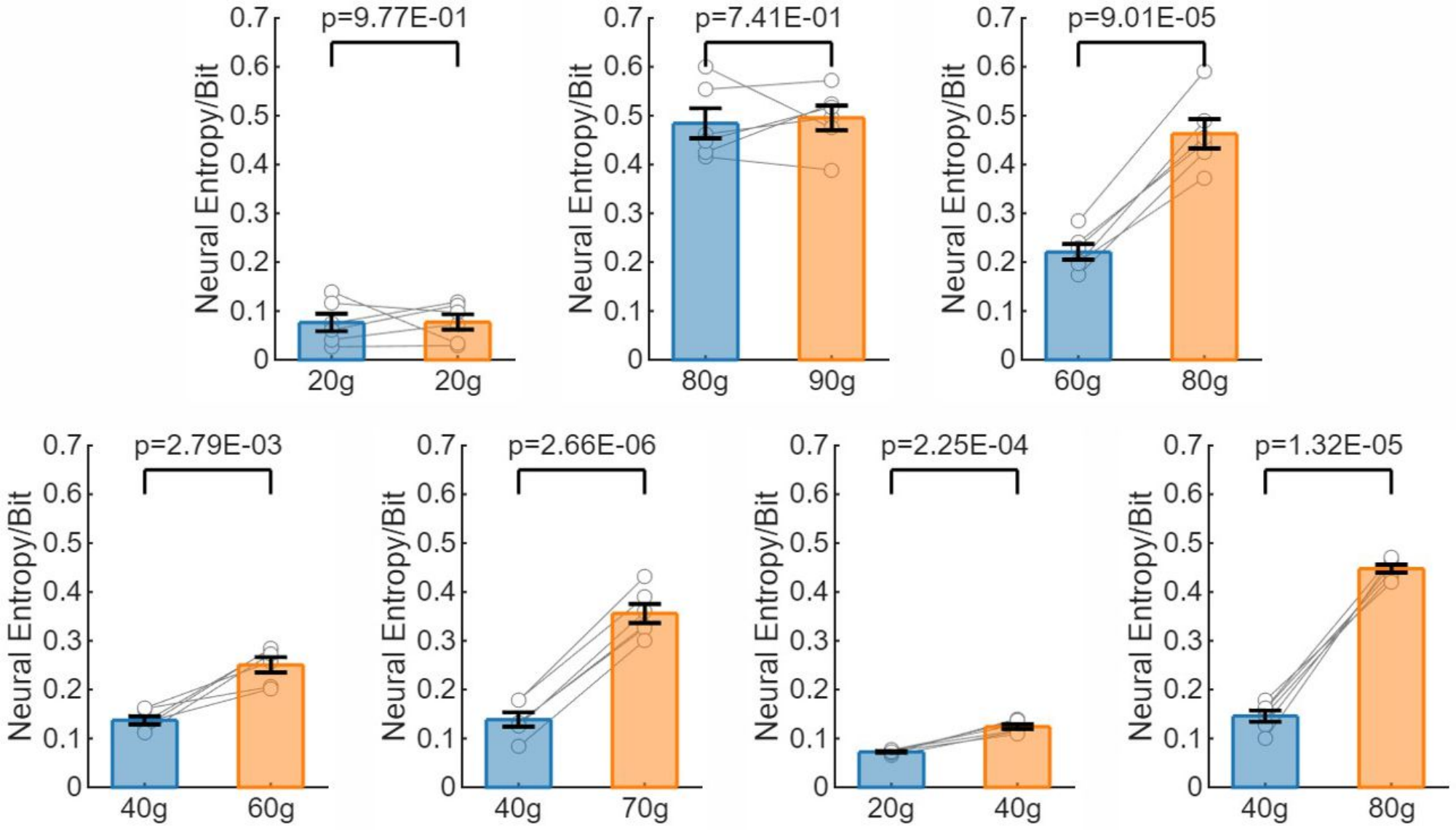
p=9.77E-01
Neural Entropy/Bit
0.7
0.6
0.5
0.4
0.3
0.2
0.1
0
20g
20g
p=7.41E-01
Neural Entropy/Bit
80g
90g
p=9.01E-05
Neural Entropy/Bit
60g
80g
p=2.79E-03
Neural Entropy/Bit
40g
60g
p=2.66E-06
Neural Entropy/Bit
40g
70g
p=2.25E-04
Neural Entropy/Bit
20g
40g
p=1.32E-05
Neural Entropy/Bit
40g
80g

Extended Data Fig. 16| Neural Entropy values. The Neural Entropy values associated with different amounts of food. Two-tailed paired t-test; mean and s.e.m. are shown; dots manifest data from individual mice (N=6).

Extended Data Table 1. The amounts of food and their ratios in the quantity discrimination assay

Amounts of Food (g/g)	Ratio
40:40	1.00
80:90	1.13
50:60	1.20
30:40	1.33
20:30	1.50
40:70	1.75
40:80	2.00
20:80	4.00
15:90	6.00

Extended Data Table 2. Two-photon imaging experiments

Amounts of Food (g/g)	Number of Recorded Neurons	Duration of Synchronous Firing (s)[a]
20:20	1,002	2.03 ± 0.01
80:90	627	1.99 ± 0.02
60:80	898	1.88 ± 0.01
40:60	1,023	1.76 ± 0.01
40:70	791	1.99 ± 0.01
20:40	1,295	1.84 ± 0.01
40:80	935	2.04 ± 0.02
20:80	807	2.06 ± 0.02

[a] Values are presented as mean ± s.e.m. (N=6).

Methods

Experimental model

All experimental procedures were approved by the laboratory animal resources center at Westlake University. The male mice at age of 6-8 weeks from C57BL/6J, 129, BALB/c, FVB/NJ, and $Arf^{FL/+}$ strains were used for the quantity discrimination assay. Only C57BL/6J mice were used for inhibitory chemogenetics, two-photon imaging experiments, olfactory test and novel object recognition test. Mice were housed under a 12-hour day/12-hour night cycle at 20℃-26℃ and were restrained from food for 48 hours before experiments.

The food-based assay

Each mouse was individually placed at the center of an open field arena measuring 30×30×50cm (length × width × height) for a 10-minute habituation period to acclimate to the environment (Fig. 1a). Subsequently, designed amounts of food (Lab Mice Diet) were placed at random at diagonally opposite corners of the arena. The behavior of each mouse was recorded with an overhead camera for 60 minutes. The remaining food in each container was subsequently measured to determine consumption. Recorded videos were analyzed with the DeepLabCut software, which enabled precise tracking of mouse movement[70]. Specific anatomical features, including the nose, ears and tail, were annotated for a detailed assessment of behavior. Using a customized MATLAB program, the distance of the mouse's nose to each food container was computed and used to calculate the percentage of time spent in proximity to interpret foraging preferences. In a series of experiments, different food amount ratios were tested using specific combinations, as outlined in Table 1 and Extended Data Table 1. In a set of visual deception experiment, 40g and 80g of food ratio 1:2 was used; however, conspicuity was manipulated by concealing a plastic block within the container holding 40g to simulate a similar visual volume as the 80g container.

Evaluation of Weber-Fechner law in the context of quantity discrimination

We designed various food amount ratios (Extended Data Table 1) and measured the ratios of the accumulated time mice spent in designated foraging zones. To analyze the relationship, we applied two mathematical models including polynomial regression and a sigmoid function. The data were most accurately described by a sigmoid curve (Fig. 1f). From the sigmoid curve, we derived the Weber fraction, a metric that quantifies the smallest detectable difference in stimulus intensity perceivable by the subject[38]. In this context, it was adapted to measure the discernible differences in food amounts. The inflection point of the curve, occurring at approximately 1.37 (Weber fraction value 0.37), was critical for determining this value.

Sensory input for discriminating different food amounts

Tactile deprivation was induced by carefully trimming the whiskers of the mice 10 minutes prior to testing[71]. Transient anosmia in the mice was induced by administering 100μl of 5% $ZnSO_4$ into each naris 24 hours before conducting the assay or olfactory test[72]. Optic nerve damage was induced by crushing the optic nerve 24 hours before testing[73], and a mutation in the *Pde6b* gene attributed to the early onset retinal degeneration specifically in the FVB/NJ mice[74]. Transient expression of Arf in the *Cdkn2a* locus resulted in aberrant postnatal proliferation in the eye and subsequent blindness in the $Arf^{FL/+}$ mice[75].

Olfactory test

The olfactory test for rodents comprises two distinct phases[76]. During the first phase (P1), containers with swabs soaked in water, which served as nonsocial cues, were placed at opposite corners of the open field arena. Subsequently, in the second phase (P2), one of the water-soaked swabs was replaced with a swab permeated with urine, providing a social olfactory cue (Extended Data Fig. 4). Mice were allowed to explore freely and detect olfactory cues for a period of 10 minutes during both P1 and P2. The movement of individual mice was analyzed similarly to that in the food quantity discrimination assay. To evaluate olfactory preference in the mice, a Preference Index (PI) was calculated by measuring their discrimination between the nonsocial and social olfactory stimuli. The PI is determined by the ratio of the difference to the sum of the accumulative time spent in the zones with social or nonsocial cues. A positive PI value indicated an individual mouse's interest in social cues.

Stereotaxic viral injection, inhibitory chemogenetics, and two-photon imaging

Mice were positioned on the stereoscopic positioning instrument after deep anesthesia induced by 1.5 to 2.5% isoflurane in oxygen[77]. The skull's fascia was removed with 4% phosphate-buffered saline following the incision of the mouse scalp. The bregma point served as the coordination origin for identifying the virus injection locations in the POR/aITC (AP: -3.00mm; ML: ±4.3mm: DV: 0.35mm), or the PPC (AP: -2.00mm; ML: ±1.6mm: DV: 0.35mm), or the PFC (AP: 2.43mm; ML: ±0.4mm: DV: 1.20mm)[50,78,79].

For experiments involving reverse inhibitory chemogenetics, a total of 200nl AAV9-hSyn-hM4Di-mCherry ($1\times10^{13} GC/ml$) virus was slowly injected at a rate of 50nl/min into the bilateral regions of the specific cortex regions[77]. The quantity discrimination behavior or the novel object recognition of individual mice was assessed 30 minutes after the intraperitoneal injection of 5.0mg/kg Clozapine N-Oxide (CNO). Following the behavioral tests, the mice underwent intracardial perfusion with 0.9% NaCl for 30 seconds and 4% paraformaldehyde for 5 minutes. Individual brains were dissected, fixed with 4% PFA for 12 hours, and subsequently dehydrated with 30% sucrose for 24 hours. The brains were then coronally sliced into 20μm sections using a cryostat (Extended Data Fig. 5)[80].

For the two-photon imaging experiments, a total of 300nl AAV9-hSyn-GCaMP6f ($1\times10^{13} GC/ml$) virus was injected into the PPC in the right hemisphere[77]. Post-virus injection, a small window of 300μm to 400μm in diameter was drilled just above the PPC and covered with a 1mm-high slide. The mice were allowed a two-week recovery period before the two-photon imaging experiments. An imaging baseplate was positioned over the slide and secured with dental acrylic. Fast high-resolution miniature two-photon microscopy (FHIRM-TPM) was employed, and its holder was mounted onto the baseplate. Images were simultaneously acquired at a predetermined frame rate during the behavior tests.

Novel object recognition test

The Novel Object Recognition test was conducted to examine the integrity of an animal's visual sensory input[81], which consisted of three distinct phases (Extended Data Fig. 6). In Phase 1 (P1), each mouse was allowed to freely explore an empty arena for 10 minutes to acclimate to the environment. In Phase 2 (P2), two identical objects (green cylinders) were placed at opposite corners of the arena, and the mice were given another 10 minutes to explore. In Phase 3 (P3), one of the familiar objects was replaced with a novel object (a yellow cube), and the mice were again provided 10 minutes to explore the arena. The analysis of the mice's exploratory behavior and the calculation

of the PI followed a protocol similar to that used in the olfactory test. A positive PI value during P3 indicated a preference for the novel object.

Two-photon imaging processing

Images of neuronal activities in the PPC layer II/III were captured in freely moving mice using FHIRM-TPM microscopy at a resolution of 600×512 pixels (487.80×416.20μm) and a frame rate of 10Hz (Fig. 2b). The two-photon images were processed using established protocols, including motion correction, noise reduction, and segmentation of neuronal components[42-44,82]. For motion correction, the NoRMCorre algorithm was employed to compensate for rigid and non-rigid translational movement[44]. Specifically, a reference frame with most activated neurons was manually selected from a subset of frames (one frame chosen from every 500, for a total of 60 frames). Each frame in the subset was aligned to this reference. The aligned frames were then averaged to create an initial reference image for the registration of the entire video. The mean projection images, both before and after registration, were illustrated (Extended Data Fig. 8a, b). Furthermore, the DeepInterpolation method, based on an encoder-decoder network with skip connections, was applied to reduce Poisson noise within individual frames[82]. The model, originally trained on high-frequency (30Hz) data, was fine-tuned using our 10Hz dataset, resulting in effective noise reduction (Extended Data Fig. 8c, d).

Segmentation of neuronal components was initially performed using established morphological methods[43]. Briefly, the two-photon images were divided into blocks of 100 frames (Extended Data Fig. 8e). For each block, both maximum and average intensity projections were calculated (Extended Data Fig. 8e). The difference between these projections was subjected to an adaptive threshold filter to generate a periodic mask containing multiple components (Extended Data Fig. 8e). These periodic masks were subsequently refined using morphological operations, such as hole filling. Subsequently, we developed a new strategy to integrate these periodic masks and automatically identify individual neuronal components, as described in a separate study. We observed that pixels belonging to the same neuronal structure were more likely to be consistently grouped into the same component across different periodic masks, providing a basis for identifying all pixels within a given neuronal component. Specifically, for any given pair of pixels, the Jaccard Index (JI) was calculated as the ratio of the number of blocks in which both pixels were classified into the same component to the number of blocks in which either pixel was identified in any component[83]. Pixels with a JI value of 0.5 or higher were grouped together, representing the spatial footprint of different regions of interest (ROI). Consequently, a temporal mask was generated (Extended Data Fig. 8f). To address potential ROI overlap, which may arise from a single neuron or from distinct neurons sharing similar imaging fields, we calculated the percentage of pixel pairs with a JI greater than 0.5 between two ROIs. A threshold of 80% or higher was used to determine whether the two ROIs originated from the same neuron. Overlapping areas were then merged to generate a spatial mask (Extended Data Fig. 8g). This spatial mask was further refined using the signal quality of individual ROIs to generate a soma mask (Extended Data Fig. 8h). This process resulted in the identification of three distinct soma-like components, which were defined as individual neurons (Extended Data Fig. 8i).

Extraction of neuronal fluorescence signal

Similar to the processing of two-photon images, neuronal signal extraction also followed established protocols[43,84,85]. Briefly, the initial fluorescence signal of any

given ROI in the spatial mask was calculated by the mean intensity of all associated pixels in each frame (Extended Data Fig. 9a, b). The neuropil fluorescence was estimated by averaging the intensities of an equivalent number of surrounding pixels (Extended Data Fig. 9a, b). An ROI was selected as neuron if its fluorescence signal exceeded the 3-sigma level of its neuropil for at least three consecutive frames (Extended Data Fig. 9b). The fluorescence signal was further refined by subtracting neuropil contamination and removing polynomial trend. Next, a baseline filter was applied to normalize the fluorescence signal (Extended Data Fig. 9c, d). This process resulted in the calcium signal, expressed as $\Delta F/F$, where ΔF represents the fluorescence change from the baseline (Extended Data Fig. 9e). In the calcium signal, positive or negative transients were identified by isolating segments of the signal that exceeded the baseline by more than two-sigma and persisted for a minimum duration of three consecutive frames[84]. The sigma value was determined separately: for positive transients, using measurements below the baseline; for negative transients, using measurements above the baseline[84,86]. Neurons exhibiting a positive-to-negative transient ratio greater than ten were selected for further analysis. Finally, the event signal was extracted from the calcium signal (Extended Data Fig. 9f), which was based on a frame rate of 100ms and a decay constant of 860ms[85].

Quantity discrimination decoding analysis

We conducted a detailed analysis of various neuronal features to decode the quantity discrimination behavior in mice. These features were calculated for either individual neurons or neuronal population within the PPC as described below. Notably, neurons located at the edges of the image were excluded to ensure accurate decoding.

Event Definition: We identified two distinct behavioral events where a mouse transitioned between foraging zones (Fig. 2c). For each event, we measured and analyzed the time spent in each zone (Extended Data Fig. 7b). Specifically, we assigned normalized time units to different behavioral states: 20 units for time spent in the zone containing more food (*e.g.*, 80g), 10 units for time in the zone with less food (*e.g.*, 20g), and 5 units for transitional periods between zones (Fig. 3b).

Neurons with preferential activities: We measured the activities of individual neurons when the animal was located in the foraging zone for the specific amount of food. Specifically, the average firing magnitude (FM) and the average firing rate (FR) per frame were assessed for each neuron. For animals presented with a specific amount of food, the neurons with preferential activities (FM or FR) were identified at a given time throughout the 60 min observation period (Extended Data Fig. 10a-c). To determine whether preferential activities changed over time, we tracked the identities of the individual neurons and their preferential activities across time and compared the data between the beginning and ending halves. In 34 out of the 48 animals, all neurons changed preferential activities. Overall, changed preferential activities were detected in 7,352 out of the 7,378 recorded neurons (Fig. 2d-g and Extended Data Fig.10d, e).

Synchronous firing of the PPC neuronal population: Among all the fired neurons in each animal presented with a given amount of food, the average percentage of the neurons fired in the same frame or the level of synchronous firing was calculated (Table 1, Extended Data Fig. 14). For the duration of synchronous firing, the Jaccard Index (JI) similarity value greater than 0.7 in all the consecutive frames or more than 82% the same neurons fired in all the consecutive frames were used for calculation (Fig. 3a, Extended Data Fig. 12)[83].

Similarity Index: To determine whether synchronous firing patterns involved the entire PPC neuronal population or specific subsets, we calculated a Similarity Index (SI) by comparing neuronal activity across different time frames (Extended Data Fig. 13). For each neuron, we computed its firing rate during two distinct synchronous firing periods. The SI was derived by first taking the absolute difference between corresponding neuronal firing rates, then averaging these differences across all neurons. Lower SI values (approaching 0) indicate greater similarity in population activity patterns between the compared periods, suggesting consistent involvement of the same neuronal ensembles.

Neural Entropy

Claude Shannon developed Shannon Entropy (*H*) to calculate the information content[46]. Given a variable X, with possible outcomes $x_1,...,x_s$, which occur with probability $p(x_1),...,p(x_s)$, the Shannon Entropy of X is defined as:

$$H(X)=\sum_{i=1}^{s} p(x_i)\log_2^{1/p(x_i)}$$

Shannon Entropy for a single transistor

A transistor on a computer chip has on and off statuses, which store information content following Shannon Entropy, as given by:

$$H(M)=\sum_{i=1}^{2} p(M_i)\log_2^{1/M_i}=\frac{1}{2}\log_2^2+\frac{1}{2}\log_2^2=1$$

Shannon Entropy for a population of transistors

A population of transistors on a computer chip constitutes a binary coding system[87], for which the information content can be expressed as the aggregate of the Shannon Entropy across S transistors in use, as calculated by:

$$H=\sum_{M=1}^{S}\sum_{i=1}^{2} p(M_i)\log_2^{1/p(M_i)}$$

For instance, for encoding a 20-pixels or 80-pixels gray image, the corresponding Shannon Entropy value would be 160 bits or 640 bits, respectively (Fig. 4a).

Information Entropy for a single neuron

A neuron also has binary conditions of fire or rest. Given a neuron (N), with its firing frequency $p(N_1)$ and its resting frequency $p(N_2)$, its information content could be similarly calculated by:

$$H(N)=\sum_{i=1}^{2} p(N_i)\log_2^{1/p(N_i)}$$

Information Entropy for a pair of neurons

For a pair of neurons, they could fire synchronously or not (Fig. 4b). Joint Entropy is employed to quantify the information content for associated events[88]. The Information Entropy for a pair of neurons (N,M) could be calculated by:

$$H(N,M)=\sum_{j=1}^{2}\sum_{i=1}^{2} p(N_j,M_i)\log_2^{1/p(N_j,M_i)}$$

Neural Entropy for a population of neurons

For a population of neurons or a brain region, it could code information by the levels of synchronous firing of the neurons. The information content could be calculated by

the level of synchronous firing or pair-wise firing of the neurons in the population, termed as Neural Entropy (*N*). For a brain region performing a particular task (X), it has a S number of neurons in its population and the pairs of synchronous firing neurons (C_S^2). The information content could be calculated by measuring the level of synchronous firing or the average of the aggregated pair-wise firing, the Neural Entropy:

$$N(X) = \frac{p(X)}{C_S^2} \sum_{N=1}^{S-1} \sum_{M=N+1}^{S} H(N,M)$$

For instance, for presented with either a 20g or 80g of food, the corresponding Neural Entropy value would be 0.14 bits or 0.45 bits, respectively (Fig. 4b).

Data availability

All data are available in this manuscript. Codes for behavior analysis or two-photon imaging analysis are available from the authors on request.

Statistical information

In our study, we employed various statistical methods to analyze the data, including the paired t-test, the unpaired t-test, the Wilcoxon signed-rank test and the Mann-Whitney U test, all conducted as two-tailed tests. P-values from the Mann-Whitney U test were adjusted using the Benjamini-Hochberg method. P-values were reported using scientific notation and rounded to two decimal places. In our data presentation, we utilized a variety of graphical representations to effectively convey our findings. Specifically, bar graphs were employed to illustrate mean values accompanied by Standard Error of the Mean (s.e.m) as error bars, with individual data points represented as dots for clarity (*e.g.,* Fig. 1d). Additionally, violin plots were utilized to display median values along with the interquartile range (25%-75%), providing insight into the distribution of the data. The data distribution was further visualized using a kernel density estimate curve (*e.g.*, Fig. 3f). Moreover, a specific graph was used to illustrate the distribution of the original data, presented through median values and interquartile ranges (*e.g.*, Extended Data Fig. 13).

Acknowledgments

We thank Lijun Xiang and Hongyan Yang for technical assistance and the Xu lab members for discussion. This study was supported in part by the grants to TX including National Natural Science Foundation of China (U21A20201), Key Laboratory of Growth Regulation and Translational Research of Zhejiang Province (2020E10027), the Science Technology Department of Zhejiang Province (2021ZY1019, 2022ZY1005), Zhejiang Leading Innovative and Entrepreneur Team Introduction Program (2018R01003), and Westlake Laboratory of Life Sciences and Biomedicine (202208011). JKP and CSX are supported by Westlake University Predoctoral Fellowship. TX is grateful to Yale and HHMI for more than two decades of support.

Author contributions

Conceptualization, JKP and TX; Methodology, JKP; Investigation, JKP and CSX; Visualization, JKP and DY; Funding acquisition, TX; Project administration, TX; Supervision, TX; Writing – original draft, JKP and TX; Writing – review & editing, JKP and TX.

Competing interests

Authors declare that they have no competing interests.

Materials & Correspondence

Correspondence and requests for materials should be addressed to the corresponding author.

References

1 Feigenson, L., Carey, S. & Hauser, M. The Representations Underlying Infants' Choice of More: Object Files Versus Analog Magnitudes. *Psychological Science* **13**, 150–156 (2002). https://doi.org/10.1111/1467-9280.00427

2 Beran, M. J. Summation and numerousness judgments of sequentially presented sets of items by chimpanzees (Pan troglodytes). *J Comp Psychol* **115**, 181–191 (2001). https://doi.org/10.1037/0735-7036.115.2.181

3 Chacha, J. *et al.* Revisiting more or less: influence of numerosity and size on potential prey choice in the domestic cat. *Animal cognition* **23**, 491–501 (2020). https://doi.org/10.1007/s10071-020-01351-w

4 Yang, T. I. & Chiao, C. C. Number sense and state-dependent valuation in cuttlefish. *Proceedings. Biological sciences* **283** (2016). https://doi.org/10.1098/rspb.2016.1379

5 Miletto Petrazzini, M. E. & Wynne, C. D. What counts for dogs (Canis lupus familiaris) in a quantity discrimination task? *Behavioural processes* **122**, 90–97 (2016). https://doi.org/10.1016/j.beproc.2015.11.013

6 VanMarle, K., Aw, J., McCrink, K. & Santos, L. R. How capuchin monkeys (Cebus apella) quantify objects and substances. *J Comp Psychol* **120**, 416–426 (2006). https://doi.org/10.1037/0735-7036.120.4.416

7 Addessi, E., Crescimbene, L. & Visalberghi, E. Food and token quantity discrimination in capuchin monkeys (Cebus apella). *Animal cognition* **11**, 275–282 (2008). https://doi.org/10.1007/s10071-007-0111-6

8 Lewis, K. P., Jaffe, S. & Brannon, E. M. Analog number representations in mongoose lemurs (Eulemur mongoz): evidence from a search task. *Animal cognition* **8**, 247–252 (2005). https://doi.org/10.1007/s10071-004-0251-x

9 Abramson, J. Z., Hernández-Lloreda, V., Call, J. & Colmenares, F. Relative quantity judgments in South American sea lions (Otaria flavescens). *Animal cognition* **14**, 695–706 (2011). https://doi.org/10.1007/s10071-011-0404-7

10 Krusche, P., Uller, C. & Dicke, U. Quantity discrimination in salamanders. *Journal of Experimental Biology* **213**, 1822–1828 (2010). https://doi.org/10.1242/jeb.039297

11 Schaffer, A., Caicoya, A. L., Widdig, A., Holland, R. & Amici, F. Quantity discrimination in 9 ungulate species: Individuals take item number and size into account to discriminate quantities. *Cognition* **254**, 105979 (2025). https://doi.org/https://doi.org/10.1016/j.cognition.2024.105979

12 Gómez-Laplaza, L. M. & Gerlai, R. J. A. C. Can angelfish (Pterophyllum scalare) count? Discrimination between different shoal sizes follows Weber's law. *Animal cognition* **14**, 1–9 (2010).

13 Lucon-Xiccato, T., Dadda, M., Gatto, E. & Bisazza, A. Development and testing of a rapid method for measuring shoal size discrimination. *Animal cognition* **20**, 149–157 (2017). https://doi.org/10.1007/s10071-016-1050-x

14 Piffer, L., Agrillo, C. & Hyde, D. C. Small and large number discrimination in guppies. *Animal cognition* **15**, 215–221 (2012). https://doi.org/10.1007/s10071-011-0447-9

15 Agrillo, C., Dadda, M., Serena, G. & Bisazza, A. Do fish count? Spontaneous discrimination of quantity in female mosquitofish. *Animal cognition* **11**, 495–503 (2008). https://doi.org/10.1007/s10071-008-0140-9

16 Sheardown, E. *et al.* Characterizing ontogeny of quantity discrimination in zebrafish. *Proceedings of the Royal Society B: Biological Sciences* **289**, 20212544 (2022). https://doi.org/10.1098/rspb.2021.2544

17 Khatiwada, S. & Burmeister, S. S. Quantity discrimination in a spontaneous task in a poison frog. *Animal cognition* **25**, 27–32 (2022). https://doi.org/10.1007/s10071-021-01528-x

18 Balestrieri, A., Gazzola, A., Pellitteri-Rosa, D. & Vallortigara, G. Discrimination of group numerousness under predation risk in anuran tadpoles. *Animal cognition* **22**, 223–230 (2019). https://doi.org/10.1007/s10071-019-01238-5

19 Dehaene, S. *et al.* Cerebral activations during number multiplication and comparison: a PET study. *Neuropsychologia* **34**, 1097–1106 (1996). https://doi.org/https://doi.org/10.1016/0028-3932(96)00027-9

20 Dehaene, S., Dehaene-Lambertz, G. & Cohen, L. Abstract representations of numbers in the animal and human brain. *Trends in neurosciences* **21**, 355–361 (1998). https://doi.org/10.1016/s0166-2236(98)01263-6

21 Chochon, F., Cohen, L., Van de Moortele, P.-F. & Dehaene, S. Differential Contributions of the Left and Right Inferior Parietal Lobules to Number Processing. *Journal of cognitive neuroscience* **11**, 617–630 (1999). https://doi.org/10.1162/089892999563689

22 Pinel, P., Dehaene, S., Rivière, D. & LeBihan, D. Modulation of parietal activation by semantic distance in a number comparison task. *NeuroImage* **14**, 1013–1026 (2001). https://doi.org/10.1006/nimg.2001.0913

23 Ansari, D., Garcia, N., Lucas, E., Hamon, K. & Dhital, B. Neural correlates of symbolic number processing in children and adults. *NeuroReport* **16** (2005).

24 Cantlon, J. F., Brannon, E. M., Carter, E. J. & Pelphrey, K. A. Functional imaging of numerical processing in adults and 4-y-old children. *PLoS biology* **4**, e125 (2006). https://doi.org/10.1371/journal.pbio.0040125

25 Castelli, F., Glaser, D. E. & Butterworth, B. Discrete and analogue quantity processing in the parietal lobe: A functional MRI study. *Proceedings of the National Academy of Sciences* **103**, 4693–4698 (2006). https://doi.org/10.1073/pnas.0600444103

26 Kaufmann, L. *et al.* A developmental fMRI study of nonsymbolic numerical and spatial processing. *Cortex* **44**, 376–385 (2008). https://doi.org/https://doi.org/10.1016/j.cortex.2007.08.003

27 Piazza, M., Mechelli, A., Price, C. J. & Butterworth, B. Exact and approximate judgements of visual and auditory numerosity: An fMRI study. *Brain Research* **1106**, 177–188 (2006). https://doi.org/10.1016/j.brainres.2006.05.104

28 Eger, E., Sterzer, P., Russ, M. O., Giraud, A. L. & Kleinschmidt, A. A supramodal number representation in human intraparietal cortex. *Neuron* **37**, 719–725 (2003). https://doi.org/10.1016/s0896-6273(03)00036-9

29 Davis, N. *et al.* The neural correlates of calculation ability in children: an fMRI

study. *Magnetic resonance imaging* **27**, 1187–1197 (2009). https://doi.org/10.1016/j.mri.2009.05.010

30 Zacharopoulos, G., Sella, F., Emir, U. & Cohen Kadosh, R. The relation between parietal GABA concentration and numerical skills. *Scientific Reports* **11**, 17656 (2021). https://doi.org/10.1038/s41598-021-95370-3

31 Nieder, A., Freedman, D. J. & Miller, E. K. Representation of the quantity of visual items in the primate prefrontal cortex. *Science (New York, N.Y.)* **297**, 1708–1711 (2002). https://doi.org/10.1126/science.1072493

32 Nieder, A. & Miller, E. K. A parieto-frontal network for visual numerical information in the monkey. *Proceedings of the National Academy of Sciences* **101**, 7457–7462 (2004). https://doi.org/10.1073/pnas.0402239101

33 Sawamura, H., Shima, K. & Tanji, J. Numerical representation for action in the parietal cortex of the monkey. *Nature* **415**, 918–922 (2002). https://doi.org/10.1038/415918a

34 Nieder, A. The neuronal code for number. *Nature Reviews Neuroscience* **17**, 366–382 (2016). https://doi.org/10.1038/nrn.2016.40

35 Nieder, A., Diester, I. & Tudusciuc, O. Temporal and spatial enumeration processes in the primate parietal cortex. *Science (New York, N.Y.)* **313**, 1431–1435 (2006). https://doi.org/10.1126/science.1130308

36 Nieder, A. & Miller, E. K. Coding of Cognitive Magnitude: Compressed Scaling of Numerical Information in the Primate Prefrontal Cortex. *Neuron* **37**, 149–157 (2003). https://doi.org/https://doi.org/10.1016/S0896-6273(02)01144-3

37 Halberda, J. & Feigenson, L. Developmental change in the acuity of the "Number Sense": The Approximate Number System in 3-, 4-, 5-, and 6-year-olds and adults. *Developmental psychology* **44**, 1457–1465 (2008). https://doi.org/10.1037/a0012682

38 Weber, E. *De pulsu, resorptione, auditu et tactu. Annotationes anatomicae et physiologicae*. (1834).

39 Fechner, G. *Elements of psychophysics*. (1860).

40 Zong, W. *et al.* Fast high-resolution miniature two-photon microscopy for brain imaging in freely behaving mice. *Nature methods* **14**, 713–719 (2017). https://doi.org/10.1038/nmeth.4305

41 Kaszas, A. *et al.* Two-photon GCaMP6f imaging of infrared neural stimulation evoked calcium signals in mouse cortical neurons in vivo. *Scientific Reports* **11**, 9775 (2021). https://doi.org/10.1038/s41598-021-89163-x

42 Giovannucci, A. *et al.* CalmAn an open source tool for scalable calcium imaging data analysis. *eLife* **8**, e38173 (2019). https://doi.org/10.7554/eLife.38173

43 de Vries, S. E. J. *et al.* A large-scale standardized physiological survey reveals functional organization of the mouse visual cortex. *Nature Neuroscience* **23**, 138–151 (2020). https://doi.org/10.1038/s41593-019-0550-9

44 Pnevmatikakis, E. A. & Giovannucci, A. NoRMCorre: An online algorithm for piecewise rigid motion correction of calcium imaging data. *Journal of Neuroscience Methods* **291**, 83–94 (2017). https://doi.org/https://doi.org/10.1016/j.jneumeth.2017.07.031

45 Tsai, M.-Y. *et al.* A reconfigurable transistor and memory based on a two-dimensional heterostructure and photoinduced trapping. *Nature Electronics* **6**, 755–764 (2023). https://doi.org/10.1038/s41928-023-01034-7

46 Shannon, C. E. A mathematical theory of communication. *The Bell System Technical Journal* **27**, 379–423 (1948). https://doi.org/10.1002/j.1538-7305.1948.tb01338.x

47 Fechner, G. T. in *Readings in the history of psychology. Century psychology series.* 206–213 (Appleton-Century-Crofts, 1948).

48 Yang, D. *et al.* Genetic association between posterior parietal cortex and intelligence. *bioRxiv*, 2025.2003.2021.644693 (2025). https://doi.org/10.1101/2025.03.21.644693

49 Hanks, T. D. & Summerfield, C. Perceptual Decision Making in Rodents, Monkeys, and Humans. *Neuron* **93**, 15–31 (2017). https://doi.org/10.1016/j.neuron.2016.12.003

50 Lyamzin, D. & Benucci, A. The mouse posterior parietal cortex: Anatomy and functions. *Neurosci Res* **140**, 14–22 (2019). https://doi.org/10.1016/j.neures.2018.10.008

51 Carandini, M. & Churchland, A. K. Probing perceptual decisions in rodents. *Nature Neuroscience* **16**, 824–831 (2013). https://doi.org/10.1038/nn.3410

52 Wang, S., Gao, H., Ueoka, Y., Ishizu, K. & Funamizu, A. Global neural encoding of behavioral strategies in mice during perceptual decision-making task with two different sensory patterns. *iScience* **27** (2024). https://doi.org/10.1016/j.isci.2024.111182

53 Kuan, A. T. *et al.* Synaptic wiring motifs in posterior parietal cortex support decision-making. *Nature* **627**, 367–373 (2024). https://doi.org/10.1038/s41586-024-07088-7

54 Orlandi, J. G., Abdolrahmani, M., Aoki, R., Lyamzin, D. R. & Benucci, A. Distributed context-dependent choice information in mouse posterior cortex. *Nature Communications* **14**, 192 (2023). https://doi.org/10.1038/s41467-023-35824-6

55 Green, J. *et al.* A cell-type-specific error-correction signal in the posterior parietal cortex. *Nature* **620**, 366–373 (2023). https://doi.org/10.1038/s41586-023-06357-1

56 Zhong, L. *et al.* Causal contributions of parietal cortex to perceptual decision-making during stimulus categorization. *Nature Neuroscience* **22**, 963–973 (2019). https://doi.org/10.1038/s41593-019-0383-6

57 Pho, G. N., Goard, M. J., Woodson, J., Crawford, B. & Sur, M. Task-dependent representations of stimulus and choice in mouse parietal cortex. *Nature Communications* **9**, 2596 (2018). https://doi.org/10.1038/s41467-018-05012-y

58 Hwang, E. J., Dahlen, J. E., Mukundan, M. & Komiyama, T. History-based action selection bias in posterior parietal cortex. *Nature Communications* **8**, 1242 (2017). https://doi.org/10.1038/s41467-017-01356-z

59 Driscoll, L. N., Pettit, N. L., Minderer, M., Chettih, S. N. & Harvey, C. D. Dynamic Reorganization of Neuronal Activity Patterns in Parietal Cortex. *Cell* **170**, 986–

999.e916 (2017). https://doi.org/10.1016/j.cell.2017.07.021

60 Morcos, A. S. & Harvey, C. D. History-dependent variability in population dynamics during evidence accumulation in cortex. *Nature Neuroscience* **19**, 1672–1681 (2016). https://doi.org/10.1038/nn.4403

61 Harvey, C. D., Coen, P. & Tank, D. W. Choice-specific sequences in parietal cortex during a virtual-navigation decision task. *Nature* **484**, 62–68 (2012). https://doi.org/10.1038/nature10918

62 Sheng, W., Huang, X., Xie, Y., Tsakiris, M. C. & Yang, Y. Posterior parietal cortex mediates rarity-induced decision bias and learning under uncertainty. *bioRxiv*, 2024.2010.2025.620383 (2024). https://doi.org/10.1101/2024.10.25.620383

63 Posner, M. I., Weible, A. P., Voelker, P., Rothbart, M. K. & Niell, C. M. Decision Making as a Learned Skill in Mice and Humans. *Frontiers in Neuroscience* **Volume 16 - 2022** (2022). https://doi.org/10.3389/fnins.2022.834701

64 Lee, J. J., Krumin, M., Harris, K. D. & Carandini, M. Task specificity in mouse parietal cortex. *Neuron* **110**, 2961–2969.e2965 (2022). https://doi.org/10.1016/j.neuron.2022.07.017

65 Ashwood, Z. C. *et al.* Mice alternate between discrete strategies during perceptual decision-making. *Nature Neuroscience* **25**, 201–212 (2022). https://doi.org/10.1038/s41593-021-01007-z

66 Minderer, M., Brown, K. D. & Harvey, C. D. The Spatial Structure of Neural Encoding in Mouse Posterior Cortex during Navigation. *Neuron* **102**, 232–248.e211 (2019). https://doi.org/https://doi.org/10.1016/j.neuron.2019.01.029

67 Song, Y. H. *et al.* A Neural Circuit for Auditory Dominance over Visual Perception. *Neuron* **93**, 940–954.e946 (2017). https://doi.org/10.1016/j.neuron.2017.01.006

68 Goard, M. J., Pho, G. N., Woodson, J. & Sur, M. Distinct roles of visual, parietal, and frontal motor cortices in memory-guided sensorimotor decisions. *eLife* **5**, e13764 (2016). https://doi.org/10.7554/eLife.13764

69 Alamu, F., Aworinde, H. & Isharufe, W. A Comparative Study of Ifa Divination and Computer Science. *INTERNATIONAL JOURNAL OF INNOVATIVE TECHNOLOGY AND RESEARCH* **Volume No. 1**, 524–528 (2013).

70 Mathis, A. *et al.* DeepLabCut: markerless pose estimation of user-defined body parts with deep learning. *Nature Neuroscience* **21**, 1281–1289 (2018). https://doi.org/10.1038/s41593-018-0209-y

71 Welker, E. & Loos, H. V. d. Quantitative correlation between barrel-field size and the sensory innervation of the whiskerpad: a comparative study in six strains of mice bred for different patterns of mystacial vibrissae. *The Journal of Neuroscience* **6**, 3355 (1986). https://doi.org/10.1523/JNEUROSCI.06-11-03355.1986

72 McBride, K., Slotnick, B. & Margolis, F. L. Does intranasal application of zinc sulfate produce anosmia in the mouse? An olfactometric and anatomical study. *Chemical senses* **28**, 659–670 (2003). https://doi.org/10.1093/chemse/bjg053

73 Kalesnykas, G. *et al.* Retinal ganglion cell morphology after optic nerve crush and experimental glaucoma. *Investigative ophthalmology & visual science* **53**,

3847–3857 (2012). https://doi.org/10.1167/iovs.12-9712

74 Pittler, S. J. & Baehr, W. Identification of a nonsense mutation in the rod photoreceptor cGMP phosphodiesterase beta-subunit gene of the rd mouse. *Proceedings of the National Academy of Sciences of the United States of America* **88**, 8322–8326 (1991). https://doi.org/10.1073/pnas.88.19.8322

75 Gromley, A., Churchman, M. L., Zindy, F. & Sherr, C. J. Transient expression of the Arf tumor suppressor during male germ cell and eye development in Arf-Cre reporter mice. *Proceedings of the National Academy of Sciences of the United States of America* **106**, 6285–6290 (2009). https://doi.org/10.1073/pnas.0902310106

76 Zou, J., Wang, W., Pan, Y. W., Lu, S. & Xia, Z. Methods to measure olfactory behavior in mice. *Current protocols in toxicology* **63**, 11.18.11–11.18.21 (2015). https://doi.org/10.1002/0471140856.tx1118s63

77 Keiser, M. S., Chen, Y. H. & Davidson, B. L. Techniques for Intracranial Stereotaxic Injections of Adeno-Associated Viral Vectors in Adult Mice. *Current protocols in mouse biology* **8**, e57 (2018). https://doi.org/10.1002/cpmo.57

78 LaChance, P. A., Todd, T. P. & Taube, J. S. A sense of space in postrhinal cortex. *Science (New York, N.Y.)* **365**, eaax4192 (2019). https://doi.org/10.1126/science.aax4192

79 Le Merre, P., Ährlund-Richter, S. & Carlén, M. The mouse prefrontal cortex: Unity in diversity. *Neuron* **109**, 1925–1944 (2021). https://doi.org/10.1016/j.neuron.2021.03.035

80 Pinskiy, V. *et al.* A low-cost technique to cryo-protect and freeze rodent brains, precisely aligned to stereotaxic coordinates for whole-brain cryosectioning. *J Neurosci Methods* **218**, 206–213 (2013). https://doi.org/10.1016/j.jneumeth.2013.03.004

81 Antunes, M. & Biala, G. The novel object recognition memory: neurobiology, test procedure, and its modifications. *Cognitive Processing* **13**, 93–110 (2012). https://doi.org/10.1007/s10339-011-0430-z

82 Lecoq, J. *et al.* Removing independent noise in systems neuroscience data using DeepInterpolation. *Nature methods* **18**, 1401–1408 (2021). https://doi.org/10.1038/s41592-021-01285-2

83 Jaccard, P. Etude comparative de la distribution florale dans une portion des Alpes et des Jura. *ulletin del la Société Vaudoise des Sciences Naturelles* (1901).

84 Komiyama, T. *et al.* Learning-related fine-scale specificity imaged in motor cortex circuits of behaving mice. *Nature* **464**, 1182–1186 (2010). https://doi.org/10.1038/nature08897

85 Kerr, J. N. D., Greenberg, D. & Helmchen, F. Imaging input and output of neocortical networks in vivo. *Proceedings of the National Academy of Sciences* **102**, 14063–14068 (2005). https://doi.org/10.1073/pnas.0506029102

86 Dombeck, D. A., Khabbaz, A. N., Collman, F., Adelman, T. L. & Tank, D. W. Imaging large-scale neural activity with cellular resolution in awake, mobile mice. *Neuron* **56**, 43–57 (2007). https://doi.org/10.1016/j.neuron.2007.08.003

87 Hopfield, J. J. Neural networks and physical systems with emergent collective

computational abilities. *Proceedings of the National Academy of Sciences of the United States of America* **79**, 2554–2558 (1982). https://doi.org/10.1073/pnas.79.8.2554

88 Quian Quiroga, R. & Panzeri, S. Extracting information from neuronal populations: information theory and decoding approaches. *Nature reviews. Neuroscience* **10**, 173–185 (2009). https://doi.org/10.1038/nrn2578